

Article

Characterization of Biofilm Microbiome Formation Developed on Novel 3D-Printed Zeolite Biocarriers during Aerobic and Anaerobic Digestion Processes

Afroditi G. Chioti ¹, Vasiliki Tsioni ¹, Stefanos Patsatzis ¹, Eirini Filidou ² , Dimitra Banti ³ , Petros Samaras ³ , Eleni Anna Economou ¹ , Eleni Kostopoulou ¹ and Themistoklis Sfetsas ^{1,*}

¹ QLAB Private Company, Research & Development, Quality Control and Testing Services, 57008 Thessaloniki, Greece

² Laboratory of Pharmacology, Faculty of Medicine, Democritus University of Thrace, 68100 Alexandroupolis, Greece

³ Department of Food Science and Technology, School of Geotechnical Sciences, International Hellenic University, 57400 Thessaloniki, Greece

* Correspondence: tsfetsas@q-lab.gr; Tel.: +30-2310-784712

Abstract: Background: Aerobic or anaerobic digestion is involved in treating agricultural and municipal waste, and the addition of biocarriers has been proven to improve them further. We synthesized novel biocarriers utilizing zeolites and different inorganic binders and compared their efficiency with commercially available biocarriers in aerobic and anaerobic digestion systems. Methods: We examined BMP and several physicochemical parameters to characterize the efficiency of novel biocarriers on both systems. We also determined the SMP and EPS content of synthesized biofilm and measured the adherence and size of the forming biofilm. Finally, we characterized the samples by 16S rRNA sequencing to determine the crucial microbial communities involved. Results: Evaluating BMP results, ZSM-5 zeolite with bentonite binder emerged, whereas ZSM-5 zeolite with halloysite nanotubes binder stood out in the wastewater treatment experiment. Twice the relative frequencies of archaea were found on novel biocarriers after being placed in AD batch reactors, and >50% frequencies of Proteobacteria after being placed in WWT reactors, compared to commercial ones. Conclusions: The newly synthesized biocarriers were not only equally efficient with the commercially available ones, but some were even superior as they greatly enhanced aerobic or anaerobic digestion and showed strong biofilm formation and unique microbiome signatures.

Keywords: aerobic digestion; wastewater treatment; anaerobic digestion; biocarriers; zeolite; biofilm; 3D printing; 16S rRNA sequencing



Citation: Chioti, A.G.; Tsioni, V.; Patsatzis, S.; Filidou, E.; Banti, D.; Samaras, P.; Economou, E.A.; Kostopoulou, E.; Sfetsas, T. Characterization of Biofilm Microbiome Formation Developed on Novel 3D-Printed Zeolite Biocarriers during Aerobic and Anaerobic Digestion Processes. *Fermentation* **2022**, *8*, 746. <https://doi.org/10.3390/fermentation8120746>

Academic Editor: Liang Yu

Received: 30 November 2022

Accepted: 14 December 2022

Published: 15 December 2022

Publisher's Note: MDPI stays neutral with regard to jurisdictional claims in published maps and institutional affiliations.



Copyright: © 2022 by the authors. Licensee MDPI, Basel, Switzerland. This article is an open access article distributed under the terms and conditions of the Creative Commons Attribution (CC BY) license (<https://creativecommons.org/licenses/by/4.0/>).

1. Introduction

Aerobic and anaerobic digestion are two different microbial processes involved in treating agricultural and municipal waste. As their names hinder, their main difference is the presence or absence of oxygen-dependent microorganisms. Aerobic digestion, otherwise referred to as wastewater treatment (WWT), is performed by oxygen-dependent microorganisms, and the resulting outcome is the transformation of active sludge into CO₂ and H₂O through oxidation, and the organic nitrogen into NH₄⁺, which can then be further oxidized and transformed into NO₃⁻ through nitrification [1]. On the other hand, anaerobic digestion (AD), involving non-oxygen-dependent microorganisms, leads to the degradation of material waste and the generation of various gases, such as methane [2].

Specific microorganisms are essential for each type of digestion, as they facilitate waste treatment. Various studies have shown that the composition of the bacterial communities change overtime, leading to the establishment of specific dominant species during the end of the waste treatment. Specifically, by the end of the treatment in aerobic digestion, Firmicutes

are the main dominant phyla, and to a lesser extent, Bacteroidetes and Proteobacteria can also be detected [3]. Similarly, in anaerobic digestion, Firmicutes and Bacteroidetes are the most dominant phyla, while some archaea phyla can also be found in abundances, such as Methanosaeta, Methanobacterium, and Methanosarcinaceae [4].

Waste treatment takes place in bioreactors, and depending on the digestion type performed, different by-products can be produced. One way to increase productivity in bioreactors is the utilization of specific biofilm carriers, or else referred to as biocarriers. Biocarriers are usually made from inorganic (zeolite), inert (polyvinyl alcohol, PVA) or reactive organic materials (alginate), come in different shapes and have porous surfaces for the microorganisms to be attached and form a biofilm [5,6]. Biocarriers enhance the bioreactor's productivity due to the available surface increase and offer protection to the attached microorganisms from the bioreactor's forces [7]. Therefore, biocarrier materials, shapes and other factors that may influence biofilm formation, have been the focus of research.

Several factors seem to play an important role on biofilm formation, these include microbial-, environmental- and carrier-related ones. Regarding the microbial-related factors, DNA, protein and lipids from the microorganisms seem to affect their ability on carrier attachment [7]. Environmental-related factors may include the bioreactor's pH, temperature or nutrients, and the carrier-related parameters involve among others, the bioprinting technique, the shape, porosity and hydrophilicity or electrophilicity of the chosen material [8,9].

Depending on the digestion type (aerobic or anaerobic), several testing methods have been developed to examine the biocarrier's efficiency in forming biofilms. The Biochemical Methane Potential (BMP) test is one of the most standard performed in anaerobic digestion systems. It measures methane production during the bioreactor's operation time [10]. The Tissue Culture Plate (TCP), a photometric method, can be applied in both aerobic and anaerobic digestion systems and translates the measured optic density into biofilm formation percentages [11]. Finally, 16s rRNA gene sequencing can be employed to analyze the composition of microbial communities formed and cultured on the biocarrier's surface [12].

In this study, we synthesized novel biocarriers by combining zeolite and different types of clay minerals. We investigated their biofilm formation efficiency in both aerobic and anaerobic digestion systems. We also performed 16s rRNA gene sequencing to examine the formed biofilms' microbial composition.

2. Materials and Methods

2.1. Biocarrier Synthesis

For the printing paste, ceramic material ZSM-5 (Thermo Fisher Scientific Inc., Waltham, MA, United States) or 13X zeolite (Alfa Aesar, Ward Hill, MA, United States) were mixed with inorganic composite material (montmorillonite or bentonite, or halloysite nanotubes) and with organic binder. Next, a colloidal silicon/ionized aqueous solution was prepared. For the successful production of printed ceramic paste, the solid content of the paste must be more than 50% to achieve the maximum density of the material and to avoid severe shrinkage during drying and calcination. Ultimately, the colloidal silicon/ionized water was gradually mixed with the solid mixture. The finished mixture was stirred with the aid of a glass rod until it assumed the structure of a viscous paste. The paste was transferred to an iron plate and treated with a metal spatula to reduce agglomerating that occurred during its preparation. A sieve with a diameter of 45 μm was used for the complete subtraction of aggregates. The paste passed through the pores of the sieve with a metal spatula. The final agglomerate-free paste had a pore diameter of less than 45 μm .

The Bio X6 (Cellink, Gothenburg, Sweden) printer from Cellink, based on DIW (Direct Ink Writing), was used to print the biocarriers. After the manufacturing process, the paste was carefully filled into the syringe to avoid forming air bubbles. The material was then centrifuged to remove air bubbles. The syringe was then placed in the printer, where print preparation took place. Preparation steps included the creation of the 3D geometry, setting parameters such as the shape of the biocarriers, the recurring geometric pattern, the

height of each layer, the nozzle diameter, the pressure and the printing speed. The chosen geometric pattern can be described as rectilinear. The individual layers were printed in one direction, with the next layer printed perpendicular to the previous one (90°). The dimensions were 24 mm wide, 14 mm long, and 7 mm high. The density of the repeating geometric pattern was 18% (Figure S1A).

Along with the six novel 3D-printed zeolite biocarriers, four commercially available biocarriers were tested; Kaldnes K1 ring (Kaldnes Miljøteknologi, Tønsberg, Norway) made from polyethylene, sponge biocarriers made from polyurethane foam, and two sintered-glass biocarriers in two different shapes, i.e., sphere (EHEIM Substrat Pro, Deizisau, Germany) and pellet (Sera Siporax Mini Professional, Heinsberg, Germany) (Figure S1B).

2.2. Brunauer-EMMETT-TELLER (BET) Special Surface Analysis

BET analysis was performed using the Quantachrome Autosorb-1-Q analyzer model (Anton-Paar, Graz, Austria). First, the test tube used for the experiment was weighed, then the test tube was weighed together with the zeolite powder (100 mg) and finally placed in the aeration position. The test tube was covered with a heating mantle and gradually heated to 150 °C. The cooling process was completed when the pressure in the test tube reached a value of less than 0.004 mmHg. Then, the test tube was cooled down to room temperature, and the sample was weighed together with the test tube to record the total mass according to the computer after steaming. Finally, the test tube was placed in the measurement position to start the experiment.

2.3. Anaerobic Development of Biofilm

Eighteen batch reactors were used at six different operations in triplicate. 150 mL of biocarriers were incubated in 350 mL inoculum (from Biogas Lagada S.A., Thessaloniki, Greece) and 2 g of microcrystalline cellulose (Sigma-Aldrich, St. Louis, MO, United States). The inoculum used had Total Solids (TS) content of 22.79 g/L, Volatile Solids (VS) content of 14.56 g/L and Free Ammonia Nitrogen (FAN) content of 490 ppm. Methane yield was calculated daily using gas chromatography coupled to thermal conductivity detector. Based on methane yield results, the beginning and the ending of exponential phase was determined.

Day 3 was characterized as before the exponential phase, day 10 as during the exponential phase and day 25 as after the exponential phase. The commercial biocarriers were harvested at these time points and were placed in new batch reactors with cow manure as digestion substrate using 1:3 ratio for the calculation of BMP. The cow manure used, had Total Solids (TS) content of 33.81 g/L, Volatile Solids (VS) content of 28.19 g/L and Free Ammonia Nitrogen (FAN) content of 1190 ppm. Then, the formation of biofilm on novel 3D-printed zeolite biocarriers was carried out, maintaining the standardized operation procedure. 3D-printed biocarriers were harvested on day 7 and were placed in new batch reactors with cow manure as a digestion substrate for BMP calculation.

2.4. Biochemical Methane Potential (BMP) Assay

A gas measurement was taken using a syringe (gas-tight) (Sigma-Aldrich, St. Louis, MO, United States) and the composition of the produced biogas was measured using a gas chromatograph (model GC-2010plus AT, Shimadzu, Kyoto, Japan) which was equipped with a Thermal Conductivity detector (TCD) and two columns (VP-Molesieve Column, FS, ValcoBond, 5A Fused Silica 15 m length, ID 0.53 mm, df 20 µm, GC-Column, FS, ValcoPLOT HayeSep D 15 m length, ID 0.53 mm, df 20 µm, VICI, Houston, TX, United States). As the free volume of each reactor was known, the volume of methane produced was calculated based on the formula:

$$\text{mL CH}_4 = \frac{\% \text{CH}_4 \times V}{100}$$

where mL CH₄ is the daily methane production in mL/d; % CH₄ is the daily percentage of methane in the batch reactor; V is the gas phase volume of the batch reactor in mL.

2.5. Lab-Scale Wastewater Treatment Set-up and Operation

Eleven 150 mL reactors were used and fed with 100 mL sludge from a municipal wastewater treatment facility (Wastewater treatment plant, Thessaloniki, Greece). The volume of each biocarrier added was 10 mL. An aeration pump (ACO-6601, HAILEA, Guangdong, China) with an output of 2.8 L/min was used and immobilized at the bottom of each reactor. 10 mL of synthetic wastewater was fed to each reactor twice a day (per 12 h) for 32 days.

Synthetic wastewater was prepared using a heated magnetic stirrer plate (VELP Scientifica, Usmate Velate, Italy) with contents of 1000 mg/L glucose; 200 mg/L NH_4Cl ; 53 mg/L KH_2PO_4 ; 18 mg/L $\text{MgSO}_4 \cdot 7\text{H}_2\text{O}$; 7.32 mg/L $\text{MnSO}_4 \cdot \text{H}_2\text{O}$; 1.1 mg/L $\text{FeSO}_4 \cdot 7\text{H}_2\text{O}$; 240 mg/L NaHCO_3 (CHEM-LAB, Zedelgem, Belgium). This recipe gave in average COD of 918 mgO_2/L , phosphorus of 12 mgP/L , nitrogen of 65.3 mgN/L and N-NH_4 of 57.7 mgN/L .

Effluent samples from each reactor were received on days 4, 11, 19, 25 and 32 for physicochemical characterization. Before sampling, the liquid level was corrected with dH_2O , and the solids were allowed to settle for half an hour.

2.6. Biofilm Extraction

The extraction of biofilm was performed as published elsewhere [13]. Biocarriers were harvested from batch reactors or wastewater treatment reactors using aseptic conditions and washed twice by gently dipping in 5 mL sterile 1X sterile phosphate-buffered saline (PBS; Sigma-Aldrich, St. Louis, MO, United States) to remove the loosely attached planktonic bacterial cells from their surface. The remaining liquid was removed by tapping on a sterile absorbent paper (capillary action). Then, the same amount of each type of biocarriers was transferred to 10 mL 1X PBS in a 50 mL tube, and a continuous vortex for 1 min at full speed was performed. Afterwards, the tubes were transferred to a sonication bath (Elmasonic S 30 H, ELMA SCHMIDBAUER, Singen (Hohentwiel), Germany) for 2 min at 37 kHz. Finally, another round of continuous vortex for 1 min at full speed was carried out. After removing the treated biocarriers, the sonicate was concentrated by centrifugation at 3100 g for 10 min. Then, 9 mL of supernatant were discarded, and the pellet was resuspended in the remaining PBS.

To confirm that biofilm has been adequately removed, treated biocarriers were dip-washed once in sterile PBS and then transferred to 5 mL sterile BHI broth (HiMedia, Thane, India). Serial dilutions were plated on tryptone soya agar (HiMedia, Thane, India). The plates were counted the next day. Based on numerous tests, we accepted as adequate biofilm extraction a remaining 1 log cfu/mL on the treated biocarrier.

2.7. Tissue Culture Plate (TCP)

The tissue culture plate method was conducted as previously described [11]. Briefly, 100 μL of the extracted biofilm suspension was transferred to 5 mL sterile BHI broth (HIMEDIA, Thane, India) and incubated for 2 h at 37 °C. Then, 200 μL was poured into the wells of sterile flat-bottomed 96-well polystyrene tissue culture plates and incubated for 24 h at 37 °C. All tests were performed in triplicate. Washing was then performed three times for each well with 1X PBS. After that, the fixation step was done by pouring 2% CH_3COONa (CHEM-LAB, Zedelgem, Belgium) for 15 min at room temperature. Then, the plates were emptied and let to air dried for 1 h at room temperature. Subsequently, the adherent biofilm layer was stained by 0.1% crystal violet (HiMedia, Thane, India) for 15 min at room temperature. Next, the washing steps were followed. Then, the plates were, once again, air-dried and resolubilized with ethanol (95%) for 30 min. The optical density (OD) of stained adherent bacteria was determined with a Microplate Reader (MR-96A, MINDRAY, Shenzhen, China) at the wavelength of 630 nm. Formation and adherence of biofilm by isolates were analyzed and categorized relying on the absorbance of the crystal violet-stained attached cells based on Table 1 as described by [11].

Table 1. Characterization of TCP results.

Mean OD Values	Adherence	Biofilm Formation
<0.120	None	None/weak
0.120–0.240	Moderate	Moderate
≥0.240	Strong	High

2.8. Determination of Physicochemical Parameters

COD (chemical oxygen demand), total N and total *p* were measured for influent synthetic wastewater as well as the effluent using Hach LCK kits (Hach, Manchester, UK) and a HACH DR 3900 spectrophotometer (Hach, Manchester, UK) for a sample per week. Concentrations of N-NH₄, N-NO₃, N-NO₂ were measured according to standard methodologies [14] using JASCO V-630 Spectrophotometer. The concentration of Mixed Liquor Suspended Solids (MLSS) and Volatile Suspended Solids (MLVSS) were determined according to the standard methods for the examination of water and wastewater [14].

2.9. Determination of Soluble Microbial Products (SMP) and Extracellular Polymeric Substances (EPS)

SMP and EPS fractions were extracted from biofilm samples following the procedure outlined by [15,16] with modification. Briefly, the sample extracted from biocarriers from lab-scale wastewater treatment, was subsequently centrifuged at 4000 g for 5 min. The supernatant was recovered and filtered through a 0.45 µm millipore filter paper. The resulting filtrate, referred to as the SMP fraction, was then analyzed for its protein and carbohydrate content. Dubois photometric method was applied to measure their content in carbohydrates [17] in duplicate for each measurement, whereas a modified Lowry method was used to measure protein concentration [18] in triplicate for each sample because of the sensitivity of the measurement. Regarding EPS extraction, the pellet obtained after the centrifugation step was suspended in 35 mL of 0.05% (*w/v*) NaCl solution, then heated at 60 °C in a water bath for 30 min and finally centrifuged at 4000 g for 15 min. The supernatant obtained, referred to as the EPS fraction, was then analyzed for its protein and carbohydrate content as described above. Protein concentrations were calibrated with Bovine Serum Albumin (BSA, Sigma Aldrich, St. Louis, MO, United States) and carbohydrates with glucose (PanReac, AppliChem, Barcelona, Spain).

2.10. DNA Extraction and 16S rRNA Gene Amplicon Sequencing

Genomic DNA was extracted from the biofilm suspensions with the DNeasy PowerSoil Pro Kit (QIAGEN, Hilde, Germany) according to the manufacturer's instructions. The quantity and quality of the extracted DNA were then estimated using a V-630 Spectrophotometer (JASCO, Inc, Tokyo, Japan). Library preparation was performed following the standard guidelines of the 16S Metagenomic Sequencing Library Preparation protocol (Illumina™, Inc., San Diego, CA, United States). In brief, DNA was amplified using the HotStarTaq® Master Mix Kit (QIAGEN, Hilde, Germany) with the addition of the 341f/805r primer pair, which targets the bacterial and archaeal V3–V4 hypervariable regions of the 16S rRNA gene (341f 5'-CCTACGGGNGGCWGCAG-3', 805r 5'-GACTACHVGGTATCTAATCC-3'). The PCR mixture (25 µL) contained 12.5 µL of HotStarTaq Master Mix, 5 µL of each primer, and 2.5 µL of DNA (5 ng/µL). Thermal cycling conditions included an initial 3-min step at 95 °C, followed by 25 cycles of denaturation at 95 °C for 30 sec, annealing at 55 °C for 30 sec and elongation at 72 °C for 30 sec and a final extension step at 72 °C for 5 min. PCR amplicons were cleaned up by AMPure XP beads (Beckman Coulter, CA, USA) to remove unbound primers and primer dimers. Next, dual indices and Illumina sequencing adaptors were attached with an index PCR using the Nextera XT Index Kit (Illumina Inc., San Diego, CA, USA). The PCR reaction mixture (50 µL) comprised 25 µL of HotStarTaq Master Mix, 5 µL of each index, 10 µL of PCR Grade Water and 5 µL of the previous PCR product, and the cycling conditions remained the same as that of the first PCR reaction except that the number of iterative cycles was reduced to 8. Afterwards, Indexed PCR amplicons

were cleaned up using the AMPure XP beads (Beckman Coulter, CA, USA). The produced DNA libraries were quantified with the Qubit™ 4 Fluorometer (Thermo Fisher Scientific, Waltham, MA, USA), and their size was verified via a 1.5 % agarose gel electrophoresis. Equimolar concentrations of the libraries were then pooled together, and a quantitative PCR was performed using the QIAseq Library Quant Assay Kit (QIAGEN, Hilde, Germany) for library concentration evaluation. The pooled library was subsequently spiked with 25% phiX control library (Illumina Inc., San Diego, CA, USA), denatured and diluted to a final concentration of 6 pM. Sequencing was performed on an Illumina MiSeq™ platform with the MiSeq Reagent Nano Kit version 2 (500-Cycle)/MiSeq Reagent Kit version 3 (600-Cycle) chemistry for a paired-end, 2x250-bp/2x300 cycle run.

2.11. Bioinformatics

Data analysis was conducted using Quantitative Insights Into Microbial Ecology 2 (QIIME2) software, version 2022.2 [19]. The same pipeline was used in two sets of samples: 11 samples of AD experiment and 11 samples of the WWT experiment. Using DADA2 algorithm [20], Amplicon Sequence Variants (ASV) were constructed after quality-based trimming, filtering and chimera detection and removal. Taxonomic annotation of the reads was conducted by employing SILVA reference database (SSU, release 138) [21]. Phylogenetic diversity was measured using the metrics Faith's Phylogenetic Diversity and weighted and unweighted UniFrac. For alpha and beta diversity analysis, q2-diversity plugin from QIIME2 software platform was used, computing several metrics and generating principal coordinates analysis (PCoA) plots using Emperor for each beta diversity metric.

2.12. Statistics

Statistical analyses for figures were performed using Prism Software 9 (GraphPad Software, San Diego, CA, USA). Results are presented as means with standard deviation and were analyzed using nonparametric one-way ANOVA. Statistical significance was established at an alpha level of $p < 0.05$.

3. Results

3.1. The Brunauer-EMMETT-TELLER (BET) Special Surface Analysis of the Novel 3D-Printed Biocarriers

BET analysis of zeolites revealed that 13X zeolite exhibits good properties with a larger specific surface area, a larger micropores volume, and a larger diameter of the micro- and mesopores compared to ZSM-5 zeolite. The ZSM-5 zeolite exhibits good properties, having a larger total pore volume and mesopore volume than the 13X zeolite (Table 2).

The various combinations of zeolites lead to the creation of complex materials with new properties and applications. One of them was the 13X/Montmorillonite, which had a larger total pore volume and a larger mesopores' volume than the pure 13X zeolite but also had a smaller specific surface area, as well as a smaller volume and diameter of micropores. The 13X/Bentonite had larger total pores and mesopores volume than 13X, but showed a decrease in specific surface area, micropores volume and diameter.

Although the 13X zeolite had a high specific surface area, its combination with inorganic materials led to its reduction, except for 13X/Halloysite nanotubes that showed an increase in the specific surface area, the total volume of the pores, and the volume of the mesopores. However, the diameter of the micropores was smaller. Similar behavior was also displayed by the ZSM-5/Bentonite, characterized by a higher diameter value than the pure ZSM-5.

The composites with 13X and ZSM-5 zeolites showed an expected decrease in their general properties due to their lower specific surface areas and micro- and mesopore volumes. Based on BET analysis, the best complex zeolites were the 13X/Halloysite nanotubes and ZSM-5/Bentonite.

Table 2. Special surface area, pore volume and size of novel 3D-printed biocarriers compared to the values of the original materials.

	Specific Surface Area (m ² /g)	Total Pore Volume (cc/g)	Micropore Volume (cc/g)	Mesopore Volume (cc/g)	Micropore Diameter (Angstrom)	Mesopore Diameter (Angstrom)
13X	688	0.35	0.29	0.06	10.2	55
ZSM5	549	0.57	0.21	0.36	5	42
Bentonite	52	0.15	0.02	0.13	na	55
Montmorillonite	32	0.16	0.01	0.15	na	55
Halloysite Nanotubes	89	0.32	0.03	0.29	na	55 and 116
13X/Bentonite	590	0.42	0.24	0.18	9	42, 116
13X/Halloysite Nanotubes	711	0.49	0.29	0.20	9	34, 55, 97
13X/Montmorillonite	687	0.42	0.28	0.14	9	39, 54, 94
ZSM5/Bentonite	527	0.56	0.21	0.35	9,4	35, 51, 116
ZSM5/Montmorillonite	na	na	na	na	na	na
ZSM5/Halloysite Nanotubes	383	0.37	0.15	0,22	na	na

*na: not applicable.

3.2. The Effect of the Novel 3D-Printed Biocarriers on Methane Production in Anaerobic Digestion

To examine the effectiveness of the novel 3D-printed biocarriers in Anaerobic Digestion (AD) systems, we first determined the productive phase of biofilm development on their surface by harvesting them at different time intervals from batch reactors operating with inoculum at mesophilic temperature. Therefore, biocarriers were harvested on day 3 (before the exponential phase), 10 (during the exponential phase) and 25 (after the exponential phase) and were subsequently transferred to bioreactors in order to perform the BMP analysis.

BMP analysis, as shown in Figure 1, revealed that, by the end of the experiment, biocarriers that were harvested on day 10 had higher methane yields in almost all four commercial biocarriers when compared with the other two exponential stages (AD-SPHERE: Before: 245.51 mL/g VS/hour \pm 13.47, During: 257.74 mL/g VS/hour \pm 5.77 and After: 207.87 mL/g VS/hour \pm 6.50, Before vs. After $p < 0.0001$, During vs. After $p < 0.0001$; Figure 1A; AD-PELLET: Before: 303.95 mL/g VS/h \pm 34.99, During: 303.89 mL/g VS/hour \pm 6.83 and After: 250.79 mL/g VS/hour \pm 9.30, Before vs. After $p < 0.0001$, During vs. After $p < 0.0001$; Figure 1B; AD-K1: Before: 263.78 mL/g VS/hour \pm 16.12, During: 268.81 mL/g VS/hour \pm 3.49 and After: 223.41 mL/g VS/hour \pm 8.76, Before vs. After $p < 0.001$, During vs. After $p < 0.0001$; Figure 1D). In the case of AD-SPONGE, biocarriers that were harvested on day 3 presented with higher methane yields (Before: 319.36 mL/g VS/hour \pm 35.21, During: 277.59 mL/g VS/hour \pm 9.03 and After: 253.89 mL/g VS/hour \pm 8.04, Before vs. After $p < 0.0001$, During vs. After $p < 0.0001$; Figure 1C). By placing them all together, we found that the AD-PELLET resulted in higher CH₄ production (Supplementary Figure S2), and therefore we proceeded with comparing the total methane production of the novel 3D-printed biocarriers with this commercially available one.

BMP analysis of the novel 3D-printed zeolite biocarriers that were pre-incubated in batch reactors with inoculum for biofilm development did not show a significant difference by comparing inorganic binders (Figure 2A,B). However, when combined (Figure 2C), both AD-13X-M and AD-ZSM5-B revealed their superiority against the commercially available AD-PELLET (AD-13X-M: 316.60 mL/g VS/hour \pm 2.51, $p < 0.01$, AD-ZSM5-B: 319.03 mL/g VS/hour \pm 4.68, AD-PELLET: 299.48 mL/g VS/hour \pm 6.69, $p < 0.001$).

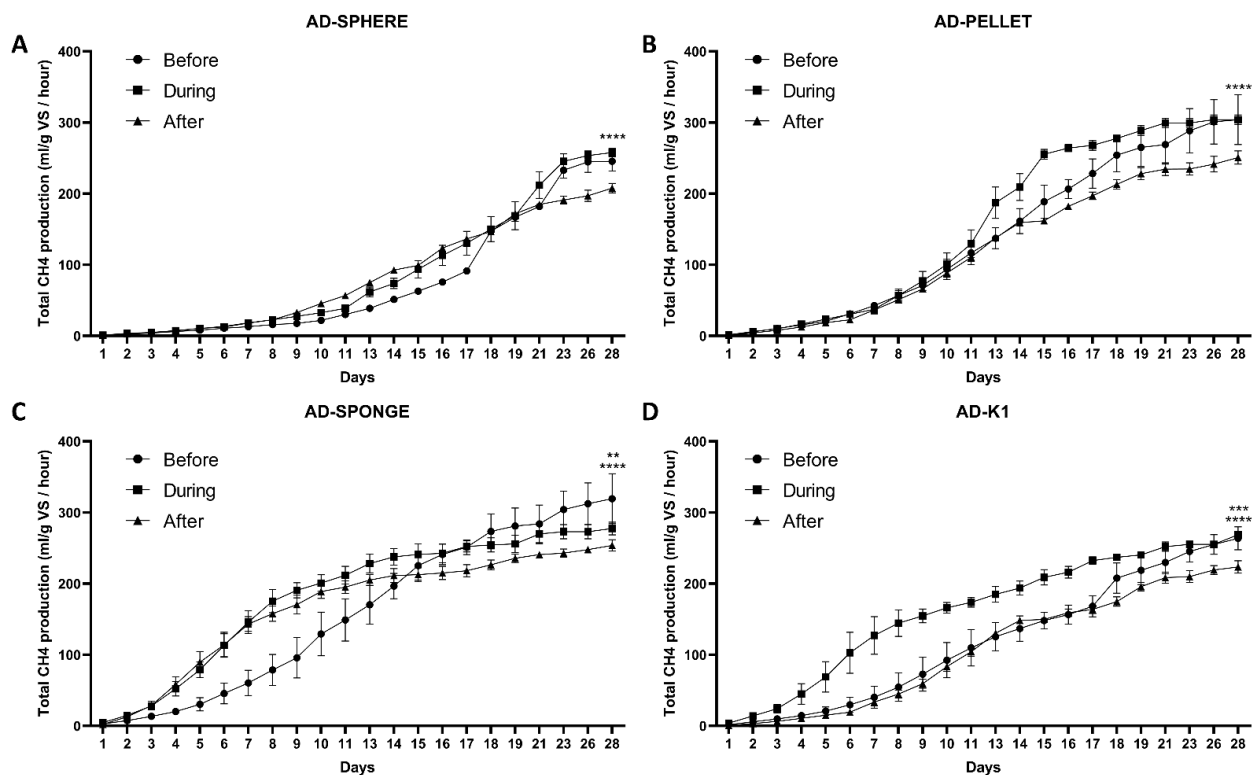


Figure 1. Total CH₄ production of commercial biocarriers on day 3 ‘Before’ exponential phase, day 10 ‘During’ exponential phase, day 25 ‘After’ exponential phase. (A) Total CH₄ production of AD-SPHERE, (B) Total CH₄ production of AD-PELLET, (C) Total CH₄ production of AD-SPONGE, (D) Total CH₄ production of AD-K1. **** $p < 0.0001$; *** $p < 0.001$; ** $p < 0.01$. $n = 3$.

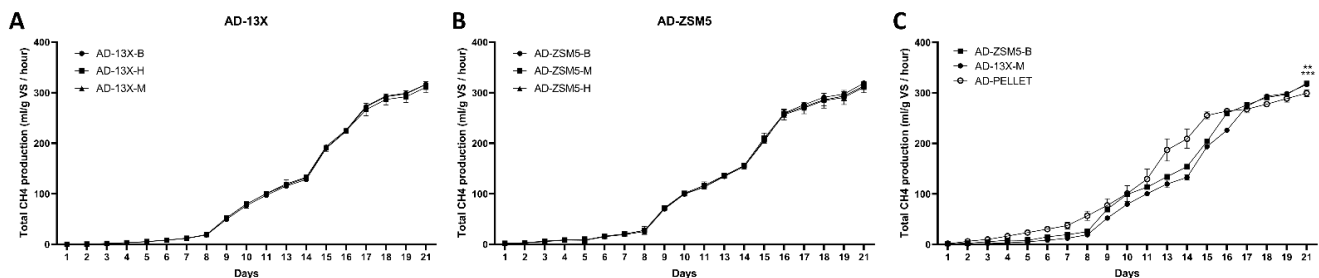


Figure 2. BMP test results of novel 3D-printed zeolite biocarriers: (A) 13X zeolite, (B) ZSM-5 zeolite, (C) mixed plot of AD-13X-M biocarrier, AD-ZSM-5-B biocarrier and AD-PELLET. *** $p < 0.001$; ** $p < 0.01$. $n = 3$.

3.3. The Effect of the Novel 3D-printed Biocarriers on Wastewater Treatment in Aerobic Digestion

When commercial and novel 3D-printed zeolite biocarriers were tested in wastewater treatment, the evaluation of the results for selecting the best WW-biocarrier was more complicated. WWT does not have an end product, like methane, that we could measure its concentration and make conclusions. So, various physicochemical parameters were evaluated weekly for a better understanding of the effectiveness of the process.

Plotting the results of commercial biocarriers, we noticed a $60.1 \pm 4.6\%$ reduction of COD during the five weekly measurements of the effluent of the reactor with WW-SPHERE, followed by WW-SPONGE with a $46.4 \pm 9.4\%$ reduction and WW-PELLET with a $34.2 \pm 1.6\%$ reduction while WW-K1 managed to reduce COD only by $10.6 \pm 8.2\%$ similarly with the reduction appeared in the control reactor where no biocarriers were used (Figure 3A). The reduction of phosphorus (P) was judged by the least squares lines slope of the results since the synthetic waste used as feed did not attribute to the overall phosphorus concentration in the WWT reactors. WW-SPHERE seemed to perform better in

phosphorus removal, followed by WW-K1, WW-SPONGE and WW-PELLET (Figure 3B). According to our measurements, only WW-SPHERE effectively reduced the added nitrogen (Figure 3C). Commercial biocarriers reduced N-NH₄ by 45% (WW-K1) to 72.2% (WW-SPHERE) (Figure 3D). Again, their nitrification potential was judged by the slope of the least squares lines of the results where WW-SPHERE contributed to N-NO₃ and N-NO₂ increase (Figure 3E,F).

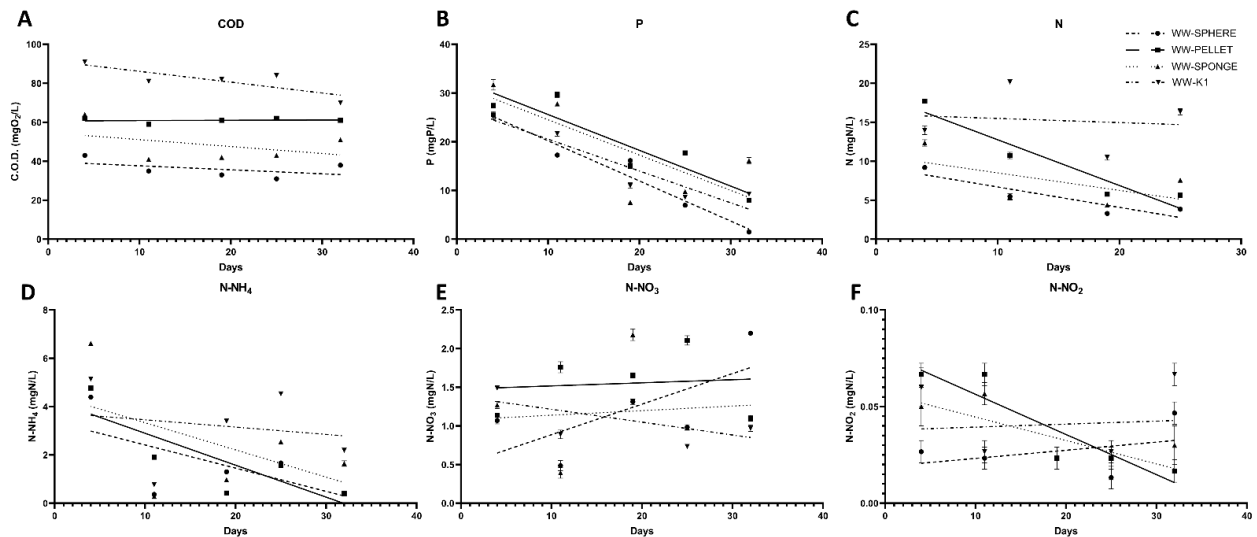


Figure 3. Variation of physicochemical parameters during WWT experiment using commercially available biocarriers. (A) COD, (B) P, (C) N, (D) N-NH₄, (E) N-NO₃, (F) N-NO₂.

For WW-13X 3D-printed zeolite biocarriers, we noticed the inadequate sedimentation of sludge due to the flotation of biocarriers. Therefore, we did not observe COD (Figure 4A) or nitrogen reduction (Figure 4C). Moreover, the concentration of N-NO₃ and N-NO₂ was not as high as expected (Figure 4E,F). However, WW-13X reduced N-NH₄ by 39.2 to 51.1% (Figure 4D) and seem to reduce sludge phosphorus (Figure 4B). Although the technical issues, WW-13X-B followed by WW-13X-H stood out between WW-13X (Figure 4).

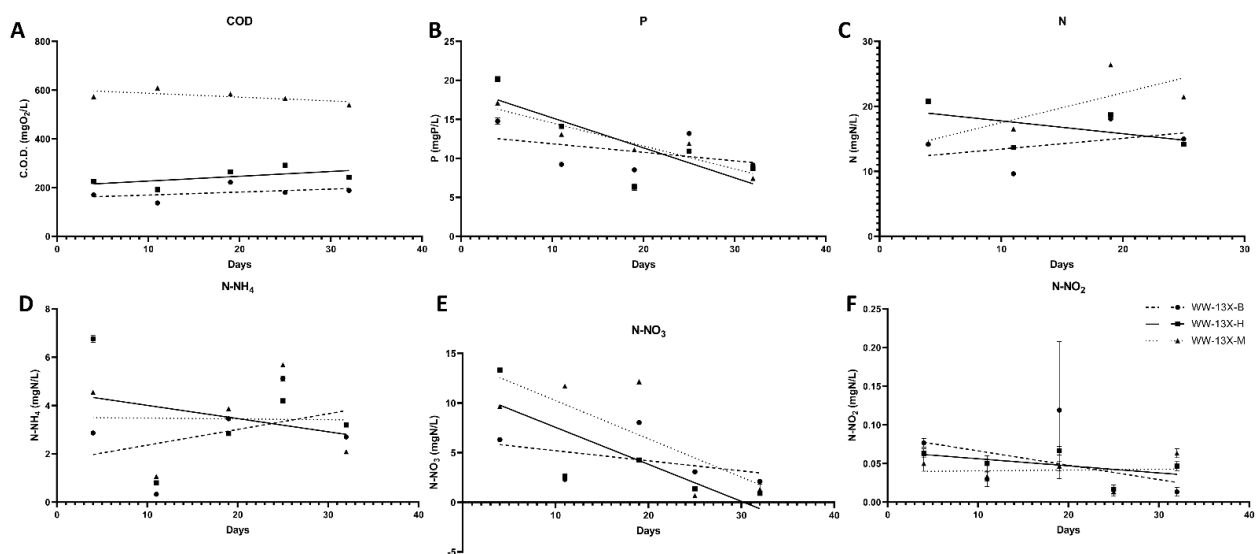


Figure 4. Variation of physicochemical parameters during WWT experiment using 3D-printed 13X biocarriers. (A) COD, (B) P, (C) N, (D) N-NH₄, (E) N-NO₃, (F) N-NO₂.

The evaluation of WW-ZSM-5 biocarriers during our experimental conditions showed the superiority of WW-ZSM5-H (Figure 5). There was a $46.6 \pm 8.9\%$ reduction of COD

(Figure 5A) and a $84.5 \pm 7.9\%$ reduction of $N-NH_4$ (Figure 5D) in the effluent of the reactor with WW-ZSM5-H, but the concentration of $N-NO_3$ and $N-NO_2$ was not as high as expected (Figure 5E,F). Moreover, WW-ZSM-5 biocarriers reduce sludge phosphorus (Figure 5B) but failed to adequately removed nitrogen (Figure 5C).

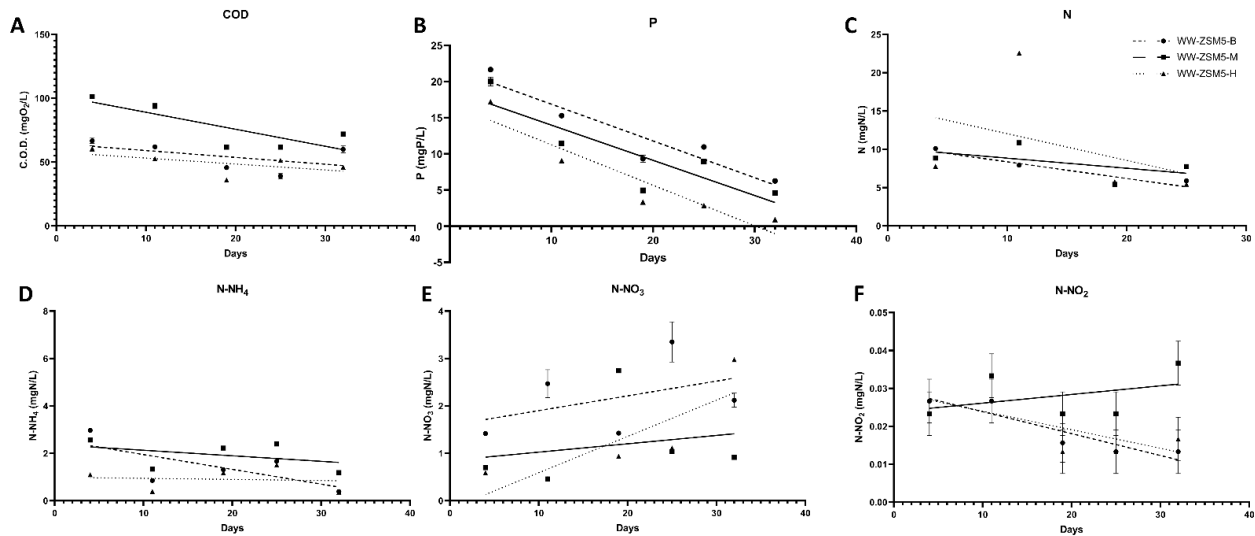


Figure 5. Variation of physicochemical parameters during WWT experiment using 3D-printed ZSM-5 biocarriers. (A) COD, (B) P, (C) N, (D) $N-NH_4$, (E) $N-NO_3$, (F) $N-NO_2$.

Plotting the 3D-printed biocarriers that stood out, together with the WW-SPHERE and the WW-CONTROL, we noticed that WW-ZSM5-H contributes equally with the WW-SPHERE in the WWT and is better than the control. Interestingly, $N-NH_4$ decreased noticeably in all reactors with biocarriers (Figure 6). Regarding the pH values, there was a slight drop in all reactors except the reactor with WW-ZSM5-M (data not shown).

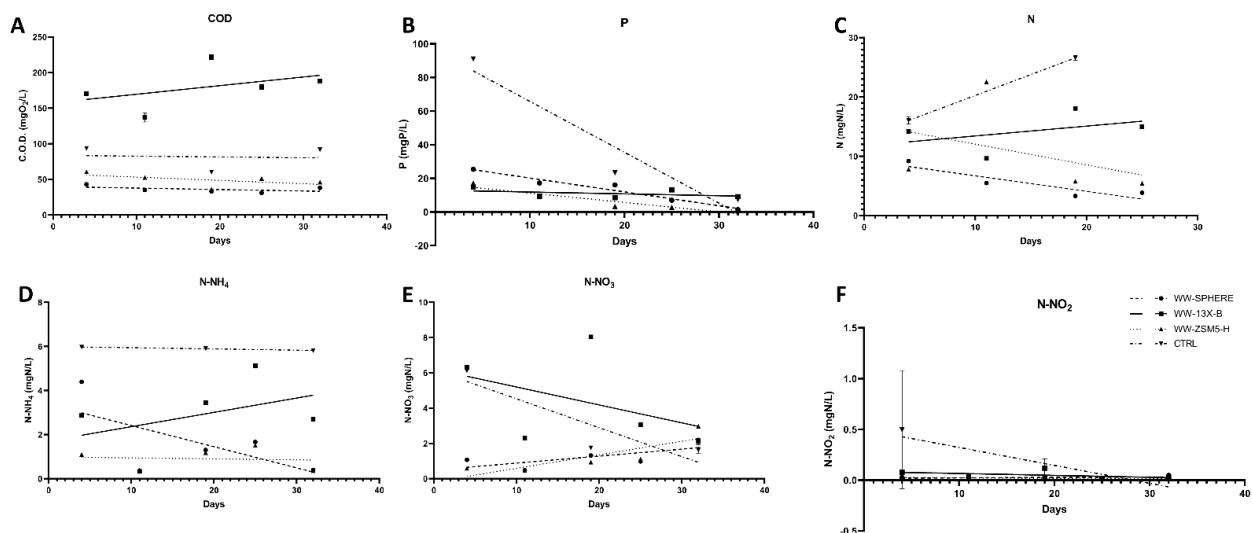


Figure 6. Effect of WW-SPHERE, WW-13X-B and WW-ZSM5-H on critical physicochemical parameters of WWT comparing with control reactor. (A) COD, (B) P, (C) N, (D) $N-NH_4$, (E) $N-NO_3$, (F) $N-NO_2$.

3.4. The Effect of the Novel 3D-Printed Biocarriers on Biofilm Composition and Formation

SMP and EPS parameters reflect the tightly and loosely bound components of biofilm composition, respectively. SMP and EPS together provide information for biofilm size, whereas EPS alone reveals the adherence of biofilm on the biocarrier [22]. When compared

with each other (Figure 7), the results revealed tightly bound biofilm and a larger amount of biofilm on K1 biocarrier (EPS proteins: 34.84 mg/g TSS \pm 20.02 and EPS carbohydrates: 4.67 mg/g TSS \pm 0.11), which was statistically significant when compared to WW-ZSM5-H (Figure 7A, $p < 0.01$), WW-ZSM5-M (Figure 7A, $p < 0.05$) or WW-ZSM5-B (Figure 7C, $p < 0.05$). Next followed the WW-SPONGE (EPS proteins: 13.37 mg/g TSS \pm 1.78 and EPS carbohydrates: 4.60 mg/g TSS \pm 1.40), which was also found statistically significant when compared to WW-ZSM5-H (Figure 7A, $p < 0.01$), WW-ZSM5-M (Figure 7A, $p < 0.05$) or WW-ZSM5-B (Figure 7C, $p < 0.05$). A large amount of biofilm, but loosely bound, was detected on WW-ZSM5-H (SMP proteins: 27.1 mg/L \pm 1.08 and SMP carbohydrates: 10.22 mg/L \pm 0.69), which was statistically significant when compared to WW-SPONGE (Figure 7B, $p < 0.01$), WW-PELLET (Figure 7B, $p < 0.05$), WW-K1 (Figure 7B, $p < 0.01$) or WW-SPHERE (Figure 7D, $p < 0.05$), but no other biocarrier differed significantly.

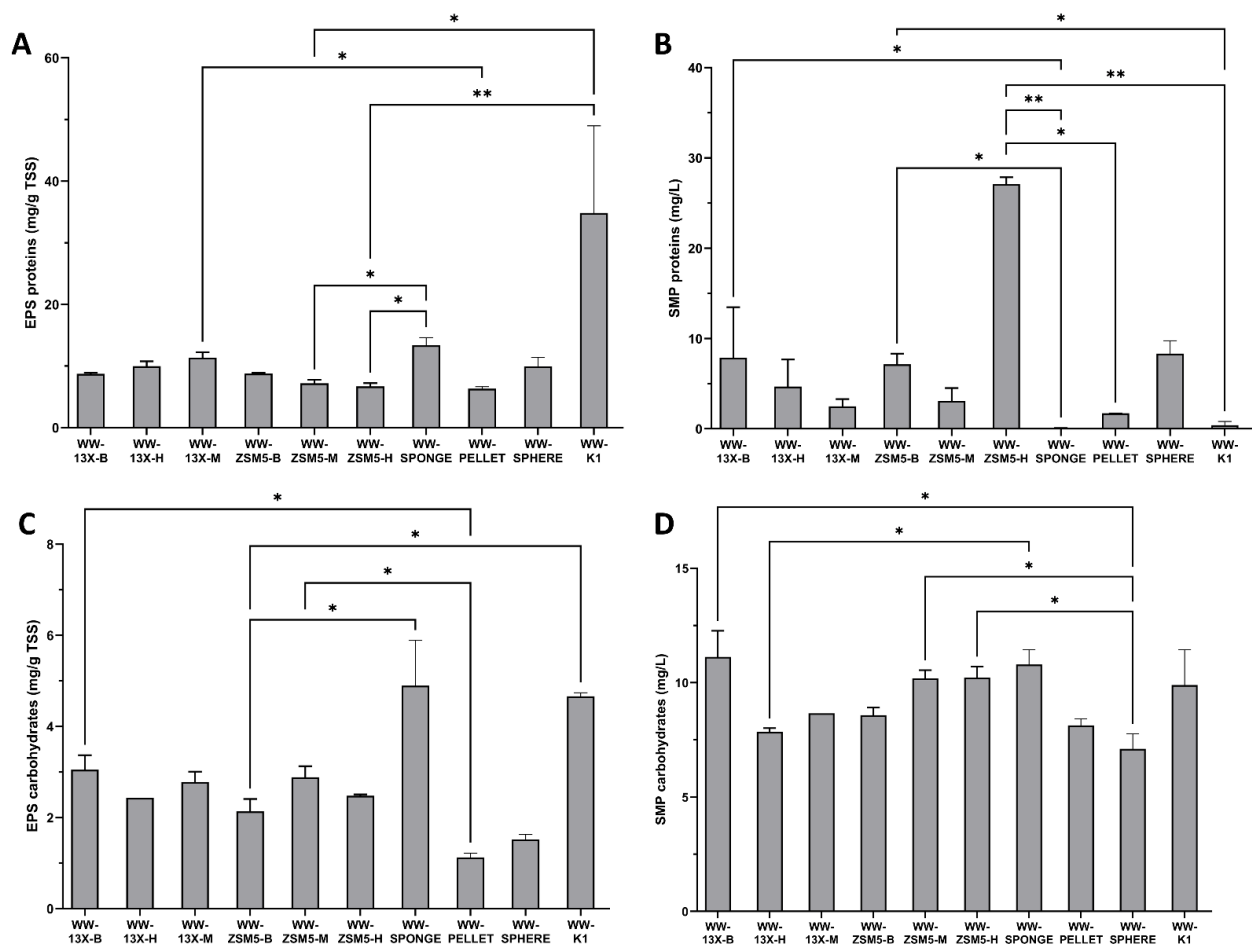


Figure 7. Bar diagrams of Soluble Microbial Products (SMP) and Extracellular Polymeric Substances (EPS) for WW biocarriers. (A) EPS proteins, (B) SMP proteins, (C) EPS carbohydrates, (D) SMP carbohydrates. ** $p < 0.01$; * $p < 0.05$. $n = 3$.

Further analysis with the TCP method on the biofilm formation of the novel 3D-printed biocarriers revealed that AD-ZSM5-H and WW-13X-B had high biofilm formation with strong microorganism adherence (AD-ZSM5-H: 0.52 O.D. \pm 0.09; Figure 8A and WW-13X-B: 0.494 O.D. \pm 0.04; Figure 8B). Additionally, AD-ZSM5-H was found to be statistically significant when compared to AD-13X-B (Figure 8A, $p < 0.01$), AD-13X-H (Figure 8A, $p < 0.01$) and AD-13X-M (Figure 8A, $p < 0.01$), while WW-13X-B was found to be statistically significant when compared to WW-13X-H (Figure 8B, $p < 0.01$), WW-13X-M (Figure 8B, $p < 0.05$) and WW-ZSM5-H (Figure 8B, $p < 0.01$).

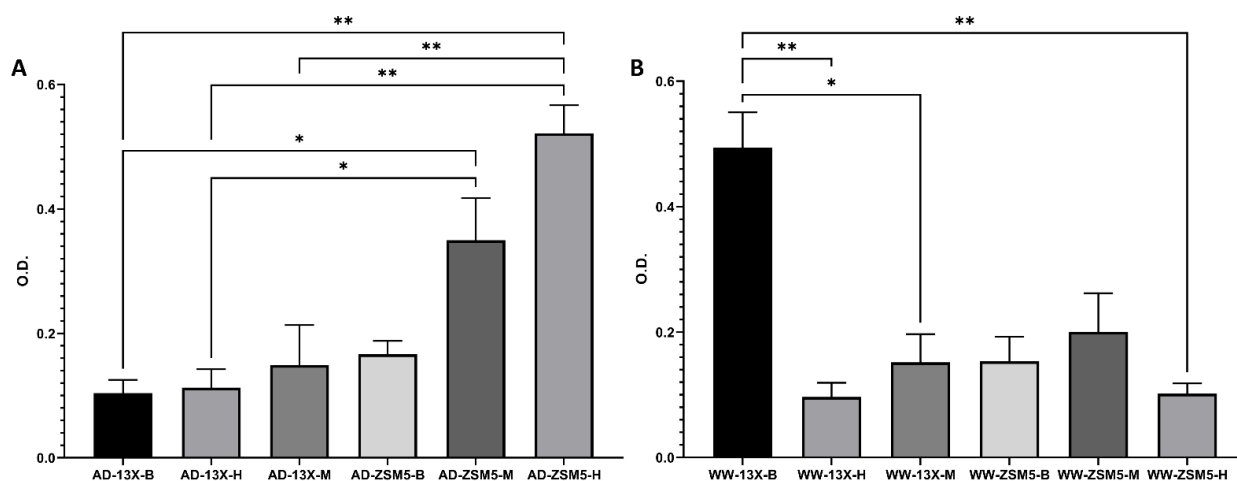


Figure 8. TCP analysis of biofilm extracted from (A) AD biocarriers and (B) WW biocarriers. ** $p < 0.01$; * $p < 0.05$. $n = 3$.

3.5. 16S rRNA Microbiome Analysis of Biofilms Developed on Biocarriers during Anaerobic Digestion

16S rRNA analysis of the anaerobically grown biofilms in the various types of biocarriers that filled the batch reactors, and also 16S rRNA analysis of a reactor sample in which no biocarriers were used (control), revealed a wealth of data. A similar number of reads were obtained for each sample, indicating a similar abundance. AD-13X-B and AD-SPHERE had the most readings, while AD-CONTROL and AD-ZSM5-H had the fewest. The data were then rigorously processed with the DADA2 tool so that only features corresponding to ASV (amplicon sequence variant) would proceed for further bioinformatics analysis. After removing noise and chimeric molecules, about 68% of the reads passed the filtering, which involved 6,535 unique features with a mean frequency of 2,549,112. More features were again found in AD-SPHERE and AD-13X-B, while fewer were in AD-ZSM5-B and AD-ZSM5-H.

We grouped the samples depending on two criteria: (a) based on biocarrier composition material i.e., 13X, glass, control (no biocarrier), pu (polyurethane) and pe (polyethylene); (b) based on whether or not biocarriers were 3D-printed i.e., 3D (3D-printed), com (commercially available), control (no biocarrier). Alpha-diversity revealed higher richness on AD-ZSM-5 than AD-13X and glass, while AD-13X showed more inhomogeneity (Figure 9A). It appears that combinations with the alumina-silica binders had a more significant effect on the biofilm composition of AD-13X than on AD-ZSM-5. Further analysis of alpha-diversity revealed that 3D-printed zeolite biocarriers differ significantly from commercial ones (p -value = $0.011 < 0.05$) (Figure 9B). Regarding beta-diversity, commercial biocarriers appeared in a different quadrant than AD-13X and AD-ZSM-5 biocarriers, while AD-CONTROL is quite far from 3D-printed and commercial biocarriers (Figure 9D).

An important observation was obtained from the abundance analysis at the first taxonomic level, with the 3D-printed biocarriers showing at least twice the relative abundances of archaea (2.2–5.4%) than the commercial biocarriers and the control (0.4–1.7%). More archaea were identified on AD-ZSM-5 (3.9–5.4%) and AD-13X-B (4%) (Table 3). The detected dominant phyla were Firmicutes with a percentage of over 50% (51.8–69.8%) in all biocarriers, except AD-ZSM-5, which ranged from 41.9–46.7%, and Bacteroidota (13.8–20.2%). On AD-ZSM-5, higher frequencies of phylum Desulfobacterota (6.7–9.9%) were detected compared to the commercial and AD-13X (<1%). AD-ZSM-5 and AD-13X-B had a higher abundance of Halobacteria (3.7–5.1%) compared to others (0.3–2%). The phylum Cloacimonadota was detected on commercial biocarriers at frequencies 4–9.9%, whereas on 3D-printed biocarriers at frequencies 1.4–3.9%. Furthermore, the phyla Synergistota and Proteobacteria were more abundant on commercial biocarriers (3.5–4.1%; 2.1–3.1%) than 3D-printed ones (1.2–2.4%; <1%) (Figure 9C).

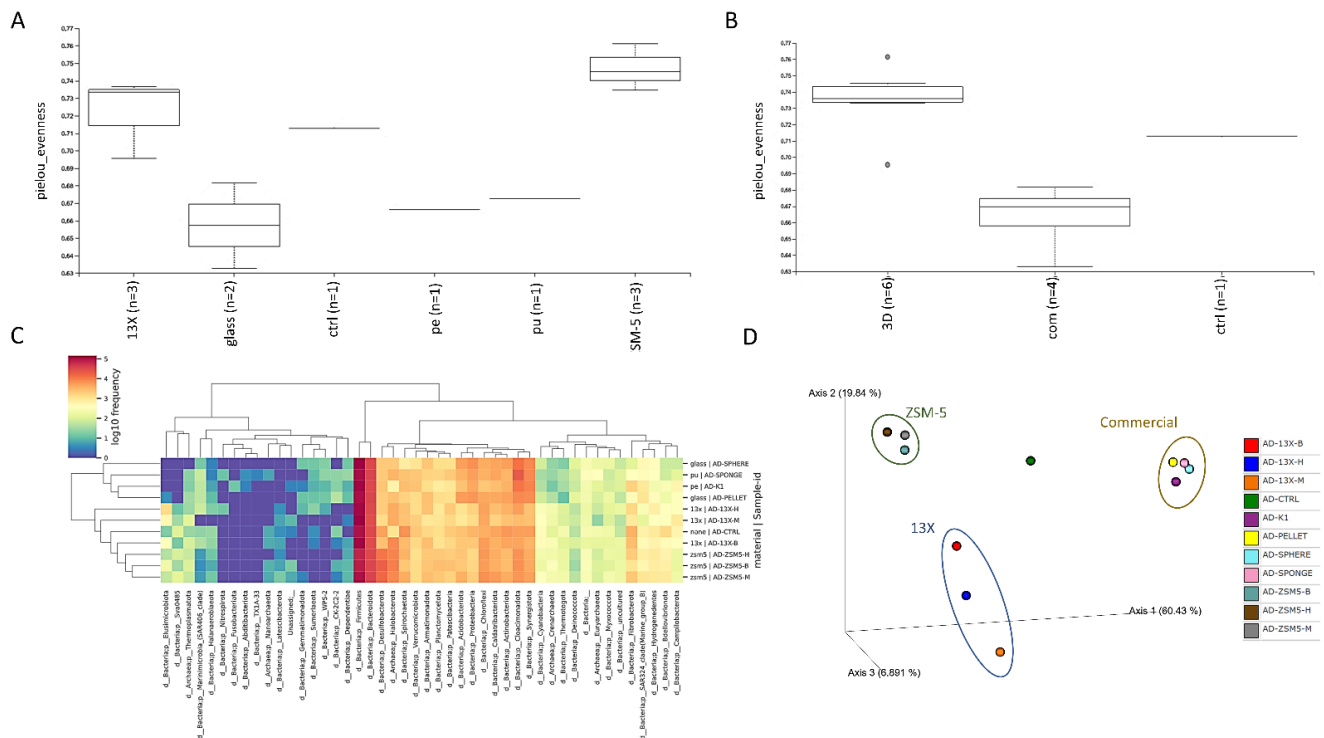


Figure 9. Core metrics results of bioinformatics of AD samples. (A). Alpha diversity boxplot of different material groups using the metric pieliou-evenness. (B). Alpha diversity boxplot of different source groups using the metric pieliou-evenness. (C). Heatmap of phyla. (D). Beta diversity plot using the metric Bray-Curtis.

Table 3. Number and percentages of ASVs assigned to bacteria and archaea domain.

Source	Material	Sample	d_Bacteria		d_Archaea		Unassigned
			ASVs	(%)	ASVs	(%)	
3D	13X	AD-13X-B	205,558	96.02	8517	3.98	0
		AD-13X-H	195,934	97.82	4371	2.18	0
		AD-13X-M	202,854	97.83	4486	2.16	8
	ZSM-5	AD-ZSM5-B	178,934	94.59	10,223	5.40	15
		AD-ZSM5-H	160,829	94.74	8936	5.26	0
		AD-ZSM5-M	207,491	96.11	8391	3.89	6
com	glass	AD-PELLET	199,781	98.62	2805	1.38	0
		AD-SPHERE	221,908	99.01	2219	0.99	0
	pe	AD-K1	215,865	99.64	772	0.36	2
none	none	AD-SPONGE	214,017	98.26	3784	1.74	0
		AD-CTRL	191,480	99.26	1423	0.74	2

Overall, the most prevalent classes were Clostridia (28.1–48.5%) followed by Bacteroidia (13.8–20.1%). AD-ZSM-5 showed a smaller abundance of Clostridia (28.1–31.2%) than the rest of the biocarriers (39.6–48.5%). In the biofilm on AD-13X-M, a relative frequency of 21.4% of the Bacilli class was detected, while on the other biocarriers Bacilli ranged around 10% and on AD-ZSM-5 around 3.4%. A relatively high abundance of the class Syntrophomonadia appeared in the 3D-printed-biocarriers (2.5–4.6%) compared to the commercial ones (<0.5%) (Supplementary Data).

The most abundant order for AD-13X and commercial biocarriers was Peptostreptococcales-Tissierellales (21.6–24.3%), which was identified to a lesser extent on AD-ZSM-5 (10.7–13.8%), in which the most abundant order was Bacteroidales (17.8–19.9%). On all 3D-printed biocarriers, the classes Syntrophomonadales and Desulfotomaculales were detected in abundances of about

4% compared to the commercial ones and the control (0.4%). Furthermore, AD-ZSM-5 presented high abundances of the order Syntrophales (6–9.3%) in contrast to all the other biocarriers examined (0.2–2%) (Supplementary Data). This result may also explain their superiority over 13X, as Syntrophales bacteria contribute to the degradation of butyrate, isobutyrate and isovalerate to produce acetic acid [23].

At family level, Peptostreptococcaceae was found to be the most abundant (16.3–23.6%) but to a lesser extent for AD-ZSM-5 (7.2–10.2%) followed by the family Clostridiaceae (5.4–11.4%). On the commercial biocarriers and in the control, the high relative abundances of bacteria of the Erysipelotrichaceae family were detected (5.5–7%) in contrast to the 3D-printed biocarriers (1.7–1.9%), whereas, on 13X biocarriers, Erysipelatoclostridiaceae family was detected to high relative frequencies (2.7–13.8%) compared to other biocarriers (<1%). Additionally, the 3D-printed-biocarriers showed high frequencies of the Syntrophomonadaceae family (2.5–4.6%), while on the commercial biocarriers and the control they were detected at rates <1% (Figure 10).

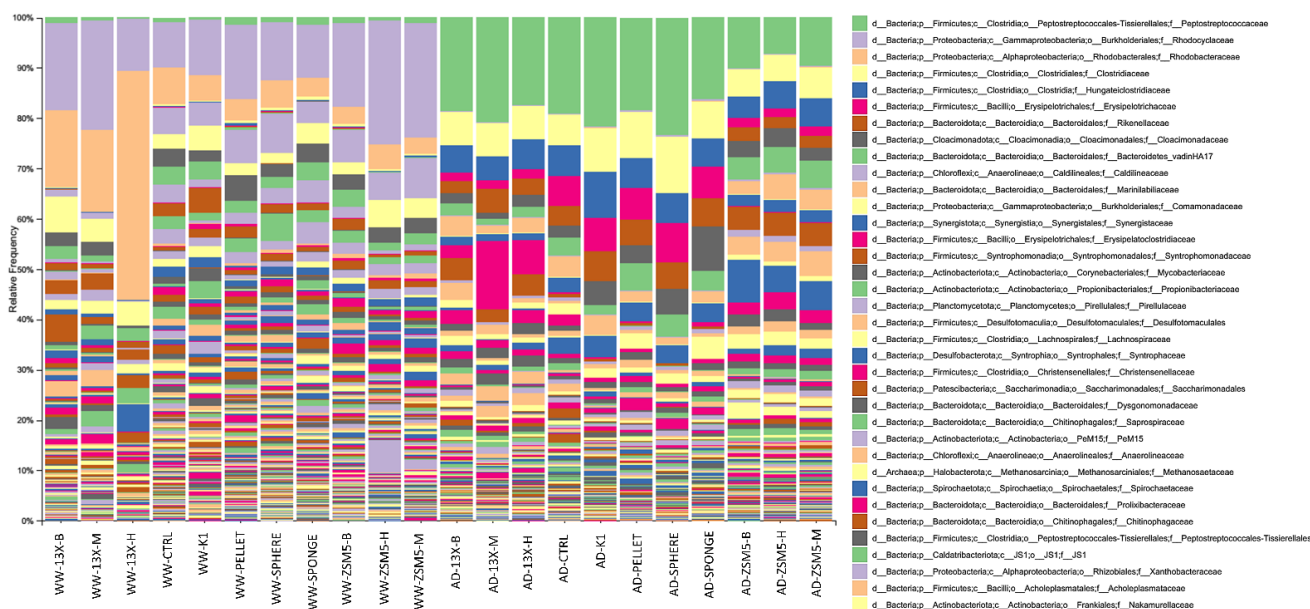


Figure 10. Bar plot of relative frequencies of identified families.

The most abundant genera, overall, were *Romboutsia* (3.5–13%), *Clostridium_sensu_stricto_1* (2.5–11.2%) and *unclassified* genera of the family Peptostreptococcaceae (3.1–10.7%). The genus *Romboutsia* covers a wide range of metabolic capacities in terms of carbohydrate utilization, single amino acid fermentation, anaerobic respiration and metabolic end products and is often identified as the most abundant genus in anaerobic digesters by 16S analysis [24]. AD-ZSM-5 showed, in addition to the above, high abundances of the genus *Syntrophus* (5.4–8.7%), *Bacteroidetes_vadinHA17* (4.3–5.4%) and *Pelotomaculum* (3.3–4.6%). Interestingly, a relative abundance of 3.3% of the hydrolytic bacteria ML635J-40_aquatic_group was identified on AD-ZSM5-B. Methanogenic archaea of the genus *Methanosaeta* were detected on AD-ZSM-5 at frequencies 2.3–2.8% with AD-ZSM-5-B showing the highest rate. As for 13X biocarriers, AD-13X-B showed frequency of *Methanosaeta* of 1.9%, slightly higher than the rest of the 13X biocarriers. Finally, among the species of methanogenic archaea, mainly uncultured species of *Methanosarcina* (1–2%) were identified (Supplementary Data).

3.6. 16S rRNA Microbiome Analysis of Biofilms Developed on Biocarriers during Aerobic Digestion

During the 16S rRNA analysis of the biofilms developed on the biocarriers used in the aerobic experiment and sludge of the wastewater reactor without biocarriers (WW-CONTROL), a wealth of data emerged. Between 212,000 and 407,000 reads were found in eight of the 11 samples, while samples WW-13X-M, WW-ZSM5-M and WW-ZSM5-H

had fewer reads. The data were rigorously processed with the DADA2 tool so that only features corresponding to ASV (amplicon sequence variant) would proceed for further bioinformatics analysis.

After removing noise and chimeric molecules, about 70% of the reads, which involved 6182 unique features with a frequency of 1,968,926, passed the filtering. In all, 245,000 to 282,000 features were found on WW-13X-B, WW-ZSM5-B, WW-CONTROL, WW-13X-H and WW-SPHERE (mentioned in descending order of feature frequency), 150,000 to 164,000 features were found on WW-PELLET, WW-K1 and 36,000 to 67,000 on WW-13X-M, WW-ZSM5- M and WW-ZSM5-H. A first observation is that biofilm was not extracted or developed in the last three samples as in the rest.

Again, we grouped the samples depending on two criteria: (a) based on biocarrier composition material i.e., 13X, glass, control (no biocarrier), pu (polyurethane) and pe (polyethylene); (b) based on whether or not biocarriers were 3D-printed i.e., 3D (3D-printed), com (commercially available), ctrl (no biocarrier). Alpha-diversity revealed a statistically significant difference between WW-13X and WW-ZSM-5 ($p = 0.05$) (Figure 11A). Higher richness and homogeneity were found on WW-ZSM-5 and glass biocarriers than WW-13X, which exhibited lower richness and inhomogeneity (Figure 11A). It appears that combinations with the alumina-silica binders had a larger effect on the biofilm composition on WW-13X than on WW-ZSM-5. Further analysis on alpha-diversity did not reveal significant differentiation between 3D-printed zeolite biocarriers and commercial ones (Figure 11B). Regarding beta-diversity, WW-13X samples tended to be in proximity, likewise WW-ZSM-5 and WW-Glass samples, while WW-K1, WW-Sponge and WW-Control were more distant from the rest of the samples (Figure 11D). Nevertheless, biocarriers made with the same material did not resemble each other as much as it would be expected.

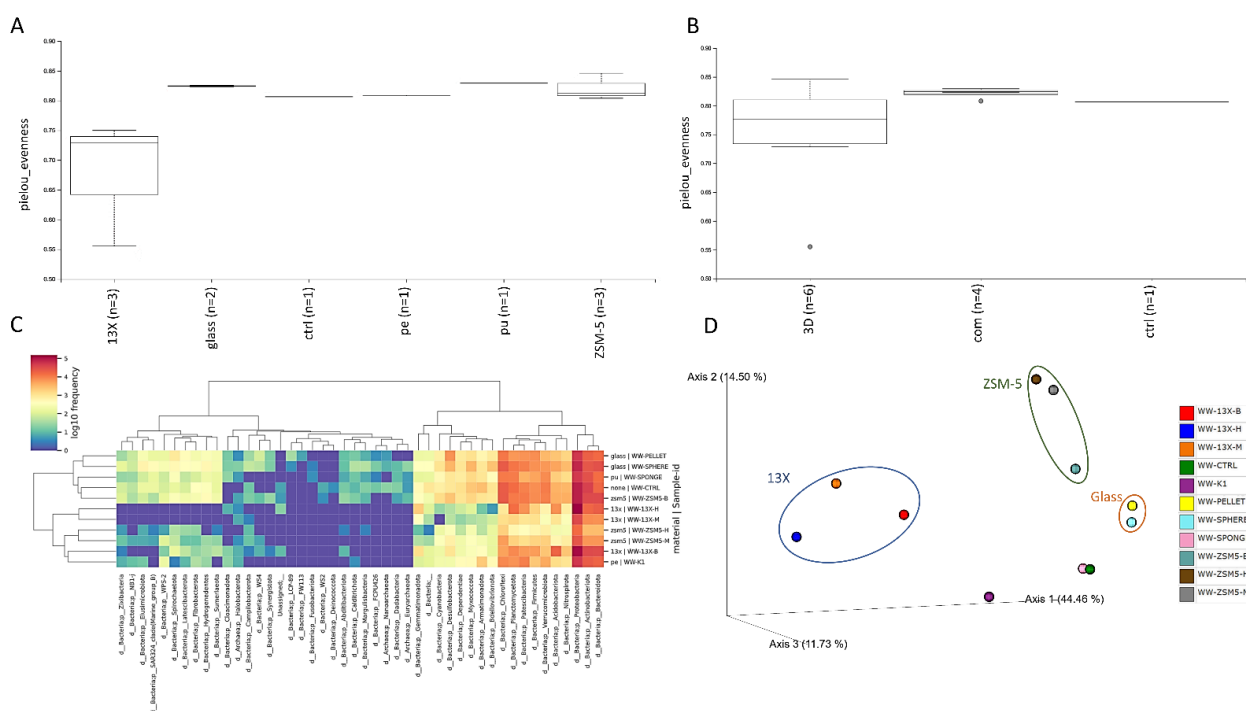


Figure 11. Core metrics results of bioinformatics of WW samples. (A). Alpha-diversity boxplot of different material groups using the metric piou-evenness. (B). Alpha-diversity boxplot of different source groups using the metric piou-evenness. (C). Heatmap of phyla. (D). Beta-diversity plot using the metric Bray-Curtis.

At domain level, all ASVs assigned to bacteria, was as expected. At phylum level, Proteobacteria (34.1–68.5%), Actinobacteria (7.4–20.5%), Bacteroidota (7.4–14.4%) and Chloroflexi (0.4–11%) were the most prevalent (Figure 11C). These phyla are often found in

laboratory-scale reactors or wastewater treatment plants [25]. WW-13X samples and WW-ZSM5-H showed >50% abundance of Proteobacteria compared to others (34.1–45.8%). On the other hand, WW-13X had a lower abundance of Chloroflexi (0.4–2.3%) and Verrucomicrobiota (0.3–1%) compared to the rest of the samples (6.5–11%; 2.3–5.8%). Other observations were that WW-K1 showed an abundance of 7.9% of the phylum Patescibacteria and WW-13X-B showed an abundance of 7.3% of the phylum Acidobacteriota while others had lower relative frequencies of these phyla (Figure 11C).

At class level, the most abundant were Gammaproteobacteria (18.5–42%), Alphaproteobacteria (10.9–49.6%), Actinobacteria (7.1–15.8%) and Bacteroidia (5.7–12.8%). It was observed that 13X was poor in Anaerolineae <2% compared to the rest of the samples (5.5–9.6%). However, 13X biocarriers were found to be richer in Alphaproteobacteria (22.9–49.6%) than the rest of the samples, with WW-13X-H showing an abundance of 49.6% while WW-ZSM5, commercial biocarriers and the control had an abundance of up to 18.1%. Twice the abundance of the class Saccharimonadia was detected in the biocarrier WW-K1 (7.8%) compared to the rest of the samples, and five times the abundance of the class Holophagae of the phylum Acidobacteriota was detected in the biocarrier WW-13X-B (5.5%) compared to the rest of the samples (Supplementary Data).

At order level, the most abundant were Burkholderiales (13.6–31.8%), Rhodobacterales (3.4–45.5) and Rhizobiales (2.5–6.4%). In fact, 13X and especially WW-13X-H showed a much higher abundance of Rhodobacterales (15.4–45.5%) and Flavobacteriales (1.5–6.7%) and a lower abundance of Caldilineales (0–1.3%) compared to the other samples (4.2–7.9%). WW-13X-H had an abundance of Gemmatales of 5.1%, and WW-ZSM-5-H had an abundance of Beggiales of 3.8%, while the other samples had <2% (Supplementary Data).

Regarding the most prevalent families of all samples, Rhodocyclaceae (9.1–25.2%) and Rhodobacteraceae (3.4–45.5%) classified respectively in the classes, Gammaproteobacteria and Alphaproteobacteria, were identified. WW-13X, and especially WW-13X-H, showed an abundance of 45.5% of Rhodobacteraceae, while the rest of the samples ranged from 3.4–7.6%. No high abundances of the Caldilineaceae family bacteria were detected in 13X (<2%) compared to the rest of the samples (4.2–7.9%). Other observations were that WW-13X-B showed an abundance of 5.3% of the Holophagaceae family, WW-13X-H showed an abundance of 5.1% of the Gemmataceae family and WW-ZSM-5-H showed an abundance of 3.8% of Beggiaaceae family, which was not identified to the rest of biocarriers other than ZSM-5 (Figure 11).

At genus level, the most significant differences were found between biofilms of the biocarriers grouped by composition material. The 13X biocarriers, and especially WW-13X-H, showed a high abundance of the genus *Paracoccus* of the family Rhodobacteraceae (42.5%), while ZSM-5 biocarriers showed a greater abundance of *unclassified* genera of the family Rhodocyclaceae (7.4–12.5%) and the genus *Zoogloea* (4.7–13%). On WW-13X biocarriers, *Zoogloea* and *Geothrix* were detected at frequencies 2.7–8.6% and 1.5–5.2%, respectively. An interesting observation was the identification of the genus *Beggiatoa* on ZSM-5 biocarriers (0.3–3.8%) which, according to the results of the aerobic experiment, worked more efficiently than WW-13X. Genus *Micropruina* of the family Propionibacteriaceae of the phylum Actinobacteria was detected in all samples (1.2 to 2.2%), except WW-ZSM-5-M, WW-13X-M (0.4%) and WW-ZSM-5-H (0.8%). Obligate aerobic bacterium *Nakamurella* belonging to Actinobacteria is another genus involved in organic carbon removal [26]. The relative abundance of *Nakamurella* was 2% in WW-13X and WW-K1 but <1% in the others. *Nitrosomonas* and *Nitrosospora* genera were expected to be detected in all samples because of their ability to oxidize ammonia [27]. However, abundance rates were not as high as expected and ranged at 1.5% with WW-13X having even less (<1%). The significant difference in relative abundance of nitrifying and heterotrophic bacteria was attributed to their competition for oxygen and space. Finally, almost all species identified were unclassified and uncultivated (Supplementary Data).

Bioinformatic analysis of all our data had some interesting results. All 13X biofilm compositions were statistically significant different from all ZSM-5 biofilm compositions

(p -value = 0,004) on the results grouped by composition material (Supplementary Figure S3A). All 13X differed significantly from control materials ($p = 0,046$), but ZSM-5 and commercial biocarriers were not significantly different using faith-pd metric on the results grouped by composition material (Supplementary Figure S3B). The beta-diversity plot showed shorter distances between AD biocarriers compared to WW biocarriers (Supplementary Figure S3C).

4. Discussion

In this study, we synthesized six new biocarriers, and compared their efficiency in aerobic and anaerobic digestion with four other commercially available biocarriers. Regarding anaerobic digestion, we found that the four out of six newly synthesized biocarriers were equivalent to the commercially available ones, as the measurable methane production was similar among them, while the other two (AD-13X-M and AD-ZSM5-B) were found to be statistically significant superior, as they lead to enhanced methane production. We also observed that four of six newly synthesized biocarriers (AD-13X-M, AD-ZSM5-B, AD-ZSM5-M and AD-ZSM5-H) had a moderate or high biofilm formation, while the other two had a weak one. Regarding aerobic digestion, we found that the WW-13X-B biocarrier resulted in a strong biofilm formation, the WW-13X-M, WW-ZSM5-B and WW-ZSM5-M in a moderate one, while WW-13X-H and WW-ZSM5-H had a weak one. In addition, we also observed that almost all biocarriers improved the physicochemical properties examined herein, with WW-13X-B and WW-ZSM5-H showing the best performance. As for the measurable EPS and SMP of proteins and carbohydrates on biofilms, we showed that the WW-ZSM5-H had the most SMP proteins compared to all other biocarriers (both new and commercially available) and WW-13X-B had the most SMP carbohydrates, respectively. Regarding the microbiome analyses, we found that all studied biocarriers had a unique microbiome signature in both anaerobic and aerobic digestion. In anaerobic digestion, all biocarriers, both new and commercially available, had a very high percentage of bacterial communities. In contrast, only the newly synthesized ones had a significant percentage of archaea ranging between 2.16–5.40%. We also performed subsequent analyses on phyla, classes, taxa, families and the genus of the microbial communities on the biocarriers from both aerobic and anaerobic digestions, and we observed that the newly synthesized biocarriers had similar microbiome signatures among them, which significantly differed from the commercially available ones.

The newly synthesized biocarriers were made with two different types of zeolite, the 13X or ZSM5. Each zeolite type was combined with three different alumina silicate binders: Bentonite, Halloysite Nanotubes or Montmorillonite. Zeolites have been long used in industries as a critical material for waste treatment processes [28]. In anaerobic digestion, its main advantages lie in decreasing the ammonia nitrogen production, a by-product that negatively affects anaerobic digestion [29], increasing the total methane production for even up to 1050% [30], and enhancing the COD removal [31]. Indeed, we also observed that the AD-13X-M and AD-ZSM5-B biocarriers, statistically significant, increased the methane concentrations when compared with other commercially available biocarriers. Montalvo et al. also observed that in bioreactors containing zeolite, among other parameters, methane production was also enhanced [32]. This finding is further supported by several other studies [33–35], suggesting that the addition of zeolites positively affects the anaerobic digestion.

Alumina silicate binders were used in the production of ceramic paste to achieve the desired viscosity [36]. In addition, they helped increase the material's porosity during calcination. The separate mixing of solid and liquid components is indicated for better homogeneity of the materials [37]. The distribution of the paste particles influenced the quality and morphology of the final product. Usually, the size of the particles in a ceramic paste is between 1 and 100 μm , with uniform distribution. For high-resolution printing attachments, it is a requirement that the particles are in a size class more minor than the diameter of the nozzle used to print the paste so that the mixture is homogeneous and

has no agglomerations. The various proportions of zeolite and alumina silicate binders were prepared with solids content ranging from 44% to 61%. The clarity level was kept low, so the final structure was mainly zeolite while maintaining good mechanical strength. The ratio of the amounts of colloidal silicon and clay was also kept constant at 2.5. The mixing ratio of zeolite and argil in the paste was 8:1, with relative amounts of 89% and 11%, respectively. The Bio X6 printer offers the ability to print a volume of $128 \times 90 \times 90$ mm ($W \times L \times H$) with an accuracy of $1 \mu\text{m}$ (arm movement). In addition, the printer allows print heads from 4°C to 250°C , which enables the viscosity of ceramic pastes to be adjusted, while the print surface can be cooled down to 4°C for better-printed structures.

The various combinations of zeolites have led to complex materials with better properties and thus better applications. Although the 13X has a high specific surface area, its combination with other zeolites leads to its reduction. The main reason for this phenomenon is that the molecules of the 13X zeolite are smaller than those of the others, which reduces the degree of its dispersion [38]. Even though 13X zeolite owns the largest specific surface area, the 13X/halloysite nano-tubes composite has a larger specific surface area, a larger total pore volume, and also a larger micro- and mesopore volume. It is generally known that nanotubes have the ability to allow the dispersion of molecules inside them, increasing the dispersion degree of the 13X zeolite [39]. In addition, the other complex materials with 13X zeolite have lower values of the special surface area and pore volume due to the ability to distribute synthetic substances materials. Despite the fact that nanotube materials have the ability to increase the degree of dispersion of the molecules of materials, in the case of ZSM-5/halloysite nanotubes, they reduce the specific surface area as well as the other parameters. This reduction in surface area may be due to the clogging of some pores by the permanent binder and the large number of total pore and mesopore volumes of ZSM-5 [40]. The composites with 13X and ZSM-5 zeolites showed an expected decrease in their general properties due to their lower specific surface areas and micro- and mesopore volumes.

Depending on the digestion type, we found that different types of biocarriers formed denser biofilms, with AD-13X-M, AD-ZSM5-B, AD-ZSM5-M and AD-ZSM5-H, and with WW-13X-B, WW-13X-M, WW-ZSM5-B and WW-ZSM5-M retrieving better results in the anaerobic and aerobic digestion, respectively. This finding suggests that both types of zeolites are equally efficient in biofilm formation, while the addition of each alumina silicate binder has a different impact depending on whether the digestion is aerobic or anaerobic. Halloysite Nanotubes and Montmorillonite were found to significantly promote biofilm formation in anaerobic digestion, while Bentonite was proven to be the most efficient in aerobic digestion, suggesting that each alumina silicate binder favors different microbial communities. Indeed, Montmorillonite has been found to better promote the survival and biofilm formation of *Arthrobacter* sp. DNS10, a bacterium involved in removing pollutants from soil [41]. In another study, Montmorillonite was again found to be more efficient in biofilm formation in an anaerobic digestion system, when compared with other clay minerals, illite and kaolinite [42]. One possible explanation for the beneficial effect of Montmorillonite in biofilm formation, came from the study of Xing et al., showing that Montmorillonite promotes the production of polysaccharides from the bacteria and thus, further enhancing the biofilm development [43]. On the other hand, Cai et al. reported that Montmorillonite could inhibit the biofilm formation of the pathogenic strain of *Escherichia coli* O157:H7 [44], suggesting that clay minerals differentially affect each bacterium. Regarding the other two clay minerals used in this study, Halloysite Nanotubes and Bentonite, little is known on their role on biofilm development, and thus our study seems to be the first in reporting their beneficial effects.

On the other spectrum, the aerobic digestion, zeolites have been proven to decrease the phosphorous and nitrogen concentrations, and to promote the sludge's settling [28]. Indeed, in our study, we observed that almost all biocarriers greatly decreased the phosphorous and nitrogen content, along with the COD, and some of them also increased the nitrate and nitrogen dioxide concentrations. Out of the six total newly synthesized biocarri-

ers, WW-13X-H and WW-ZSM5-H showed the most efficient improvement of the studied physicochemical properties. Our results are in agreement with other studies reporting that the addition of zeolite or clay minerals promote denitrification [45,46], suggesting that specific types of biocarriers favor the development of the appropriate bacterial communities for more efficient aerobic digestion. Biocarriers have been generally found to improve the physicochemical properties of the aerobic digestion [47], and in our study the ones combined with Halloysite Nanotubes proved to have a more beneficial effect when compared to commercially available biocarriers, suggesting that Halloysite Nanotubes may promote the survival and proliferation of nitrogen- and phosphorous-accumulating bacteria. Nonetheless, we also observed that in the case of the WW-13X-H biocarrier, the percentage of both nitrate and nitrogen dioxide was decreased, instead of increased, and this could be attributed to the flotation phenomena that were detected.

Regarding the EPS and SMP results on proteins and carbohydrates, we showed that the WW-ZSM5-H had the most SMP proteins compared to all other biocarriers (both new and commercially available) and WW-13X-B the most SMP carbohydrates, respectively. The EPS and SMP regulate the physicochemical and biological properties of the activated sludge and are key components of its structure, as they enable the formation of microenvironments in which the microorganisms develop. EPS is considered to form a matrix, in which microorganisms are protected, enabled to adhere on surfaces, provided with required nutrients and develop and proliferate in a more stable way [48]. More specifically, they constitute a three-dimensional biofilm network in the form of a gel, highly hydrated and often charged, in which the microorganisms are integrated and immobilized, and the percentage of extracellular polymeric components in biofilms ranges from 50–90% of the total organic matter [49]. On the other hand, SMPs are high molecular weight secreted molecules that are produced by the microorganisms and they seem to have a significant role in influencing the chemical oxygen demand (COD) and biochemical oxygen demand (BOD) during waste treatment [50]. It is speculated that an increased concentration of EPS suggests a stronger biofilm adherence [22]. Our results agree with previous studies indicating that the addition of biocarriers results in a significant increase of total EPS [51,52].

As already mentioned, the microbiome analyses revealed that all studied biocarriers had a unique microbiome signature in both anaerobic and aerobic digestion, suggesting that the materials used have different effects on the microbial communities. More specifically, in the anaerobic digestion, the percentage of bacterial communities was very high among all studied biocarriers, while only the newly synthesized ones had a significant portion of archaea. In contrast to other studies showing that the Bacteroidetes are the main bacterial phyla on the anaerobic digestion's biofilms, ranging from 41.94–71.67% [53], in our study Firmicutes were the most dominant in all biocarriers. This finding may be explained by the fact that Bacteroidetes flourish in substrates rich in lignocellulosic compounds [54,55], while the materials used in this study did not contain these compounds and, therefore, may mostly favor the populations of Firmicutes, instead of Bacteroidetes. Going even further, *Clostridium* was found to be the most profound class of Firmicutes in all biocarriers' biofilms. Previous studies have shown that *Clostridia* metabolize glucose to produce ethanol, lactic and acetic acid, CO₂ and H₂, all essential compounds for methane production [56], and microbial ecosystems with high performances seem to be mainly populated by this type of bacterial class [56]. Another interesting result of our study was the identification of the genus *Methanosaeta* of the methanogenic archaea, that has a crucial role in the production of methane through the acetoclastic pathway [57,58]. They have been identified as the main methanogenic archaea in the anaerobic digestion of bovine's manure [59], while in another study, the addition of biocarriers resulted in the increase of their population from 2% to 10.01%, enhancing at the same time methane production [60]. Another identified genus, although in less than 2%, was the one of *Methanoculleus*, which are anaerobic hydrogenotrophic methanogenic archaea, and have been also associated with enhanced methane and biogas production [61].

Regarding aerobic digestion, the phylum analysis highlighted the presence of Proteobacteria, Actinobacteria, Bacteroidota and Chloroflexi, all of which have been mainly found in laboratory-scale reactors or in sewage treatment plants [25]. It should be noted that the microbiome analysis on the family level revealed the presence of Rhodobacteraceae, which is found to prevail in the absence of nitrates [62], and Rhodocyclaceae, which is found to metabolize various chemical compounds, such as nitric ones [63]. Therefore, this finding may explain the relative low percentages of NO_2 and NO_3 found in some biocarriers' reactors. On the genus level, *Paracoccus spp.* was found in high rates on the biofilm of WW-13X biocarriers, and previous studies have underlined its crucial role in bioreactors, as through denitrification [64] it can remove potential hazardous organic compounds [65]. Another identified genus was the one of *Zoogloea*, a Gram-negative bacterium that has been found to produce EPS for floc formation, improving in this way the sedimentation, but may also cause other problems, such as foaming [66]. *Beggiatoa* was another genus that was found in abundance only on ZSM-5 biocarriers' biofilm and it has been reported to thrive in environments rich in sulfur, as it oxidizes H_2S through a process called chemolithotrophy [67]. So far, there have been identified both autotrophic and heterotrophic types of *Beggiatoa*, with the first type being mainly found in sea water and the last one mainly in fresh water, but both are associated with sulfur-enriched environments [68]. Another genus we identified was the *Micropruina*, which is implicated in the consumption of organic substrates, and specifically, it has been found that in aerobic digestion, it metabolizes glycose resulting in the accumulation of glycogen [69].

Since a large proportion of the genus analyses was attributed to unclassified or others, many others may be involved in organic carbon and nitrogen removal. In addition, the effect of the carrier size on reactor performance may be reflected by the difference in microbial communities and the relative abundance between samples. Proteins and carbohydrates in EPS also play a key role in reactor performance, as their composition and content directly affect the formation and stability of cell aggregates and their adhesion to the carrier surface [70]. It has been reported that a protein/carbohydrate ratio of 1.40 was beneficial for the growth of aerobic granular sludge [71]. Biocarriers are more like a set of many aerobic granules entrapped and immobilized by the EPS, and thus creating different microenvironments (aerobic/anoxic or aerobic/anoxic/anaerobic) distributed in the biofilm.

The 3D biocarriers with Bentonite as an inorganic binder presented a greater abundance; however, a biofilm of different microbial diversity was developed on them. Despite the successful growth of rich biofilm on WW-13X-B biocarrier, all 13X biocarriers did not perform as expected in aerobic waste treatment. It is likely that the experimental conditions hindered their actual dynamics, and especially for WW-13X-B and WW-13X-H, due to flotation phenomena. Nevertheless, the results support the superiority of WW-ZSM-5 biocarriers and especially WW-ZSM5-H. The success of WW-ZSM5-H in the laboratory aerobic waste treatment experiments, despite the low microbial abundance detected on it and the negative result in the TCP test, is likely due to the indirect support of functional microbial populations rather than as a substrate for their growth.

The inorganic binders that were used affected the 13X zeolites much more than the ZSM-5 ones and therefore a large inhomogeneity was observed between the biofilms developed on the 13X 3D-biocarriers. Judging from the homogeneity of the glass commercial biocarriers, it appears that the shape does not affect adhesion as much as the construction material. In terms of taxonomic composition, the microbiome found in ZSM-5 biocarriers was more similar to commercial biocarriers than 13X with more abundant Rhodocyclaceae (16.7–25.2%) and Caldilineaceae (5.4–7.9%) families, while the correlation between the high abundant genus *Zoogloea* on WW-ZSM5-H and the biocarrier's effectiveness, remains to be investigated.

Supplementary Materials: The following supporting information can be downloaded at: <https://www.mdpi.com/article/10.3390/fermentation8120746/s1>, Supplementary Figure S1: (A) Novel 3D-printed zeolite biocarriers. (B) Commercially available biocarriers. Supplementary Figure S2: Total CH₄ production of commercial biocarriers during the exponential phase of microorganisms forming a biofilm on their surface. AD-SPHERE: 257.74 mL/g VS/hour ± 5.76, AD-PELLET: 303.89 mL/g VS/hour ± 6.84, AD-SPONGE: 277.59 mL/g VS/hour ± 9.03, AD-K1: 268.81 mL/g VS/hour ± 3.49, Control: 274.04 mL/g VS/hour ± 5.95, AD-SPHERE vs. AD-PELLET $p < 0.0001$, AD-PELLET vs. AD-SPONGE $p < 0.05$, AD-PELLET vs. AD-K1 $p < 0.001$, AD-PELLET vs. Control $p < 0.01$. Supplementary Figure S3: Core metrics results of bioinformatics of all AD and WWT samples. A. Alpha diversity boxplot of different biocarrier composition material groups using the metric `pielou_evenness`. B. Alpha diversity boxplot of different biocarrier composition material groups using the `faith_pd`. C. Beta diversity plot using the metric Bray-Curtis, WWT samples are represented by a conical shape, and AD samples are represented by rings. Supplementary Data: csv tables of different levels of taxa.

Author Contributions: Conceptualization, T.S. and A.G.C.; methodology, V.T, D.B., S.P., E.A.E., E.K. and A.G.C.; software, A.G.C. and E.F.; validation, T.S., A.G.C. and V.T.; formal analysis, A.G.C., V.T., S.P. and D.B.; investigation, A.G.C., S.P., E.K., D.B. and T.S.; resources, T.S. and V.T.; data curation, A.G.C., T.S. and E.F.; writing—original draft preparation, A.G.C. and E.F.; writing—review and editing, T.S, P.S., E.A.E., E.K. and D.B.; visualization, E.F. and A.G.C.; supervision, T.S.; project administration, T.S.; funding acquisition, T.S. All authors have read and agreed to the published version of the manuscript.

Funding: This research was co-funded by the European Regional Development Fund of the European Union and Greek national funds through the Operational Program Competitiveness, Entrepreneurship and Innovation, under the call RESEARCH—CREATE—INNOVATE (project code: T2EDK-00362).

Institutional Review Board Statement: Not applicable.

Informed Consent Statement: Not applicable.

Data Availability Statement: The data presented in this study are available upon request from the corresponding author.

Acknowledgments: The authors wish to acknowledge Biogas Lagada SA, that provided the inoculum and feed material to be used for experimentations. The authors also wish to acknowledge Professor Thomas A. Kotsopoulos and Christos A. Tzenos from Department of Hydraulics, Soil Science and Agricultural Engineering, AUTH whose input was greatly appreciated. Finally, the authors acknowledge all staff members of Qlab P.C. for their individual roles that contributed to the implementation of this study, thank you Ioanna Dalla, Nikoleta Prokopidou, Anastasia Manavi, Georgia Dimitropoulou, Ifigenia Grigoriadou, Ioanna Christoforidou and Panagiotis Pantazis.

Conflicts of Interest: The authors declare that they have no known competing financial interest or personal relationship that could have appeared to influence the work reported in this paper.

References

1. Al-Ghusain, I.; Hamoda, M.F.; Abd El-Ghany, M. Nitrogen transformations during aerobic/anoxic sludge digestion. *Bioresour. Technol.* **2002**, *85*, 147–154. [[CrossRef](#)] [[PubMed](#)]
2. Saravanan, A.; Kumar, P.S.; Nhung, T.C.; Ramesh, B.; Srinivasan, S.; Rangasamy, G. A review on biological methodologies in municipal solid waste management and landfilling: Resource and energy recovery. *Chemosphere* **2022**, *309*, 136630. [[CrossRef](#)] [[PubMed](#)]
3. Zhang, M.; Tashiro, Y.; Ishida, N.; Sakai, K. Application of autothermal thermophilic aerobic digestion as a sustainable recycling process of organic liquid waste: Recent advances and prospects. *Sci. Total Environ.* **2022**, *828*, 154187. [[CrossRef](#)]
4. Pasalari, H.; Gholami, M.; Rezaee, A.; Esrafil, A.; Farzadkia, M. Perspectives on microbial community in anaerobic digestion with emphasis on environmental parameters: A systematic review. *Chemosphere* **2021**, *270*, 128618. [[CrossRef](#)]
5. Zhao, Y.; Liu, D.; Huang, W.; Yang, Y.; Ji, M.; Nghiem, L.D.; Trinh, Q.T.; Tran, N.H. Insights into biofilm carriers for biological wastewater treatment processes: Current state-of-the-art, challenges, and opportunities. *Bioresour. Technol.* **2019**, *288*, 121619. [[CrossRef](#)]
6. Raj Deena, S.; Kumar, G.; Vickram, A.S.; Rani Singhanian, R.; Dong, C.D.; Rohini, K.; Anbarasu, K.; Thanigaivel, S.; Ponnusamy, V.K. Efficiency of various biofilm carriers and microbial interactions with substrate in moving bed-biofilm reactor for environmental wastewater treatment. *Bioresour. Technol.* **2022**, *359*, 127421. [[CrossRef](#)] [[PubMed](#)]

7. Li, L.; He, Z.; Liang, T.; Sheng, T.; Zhang, F.; Wu, D.; Ma, F. Colonization of biofilm in wastewater treatment: A review. *Environ. Pollut.* **2022**, *293*, 118514. [[CrossRef](#)]
8. Yang, D.; Zhang, X.; Zhou, Y.; Xiu, Z. The Principle and Method of Wastewater Treatment in Biofilm Technology. *J. Comput. Theor. Nanosci.* **2015**, *12*, 2630–2638. [[CrossRef](#)]
9. Sfetsas, T.; Patsatzis, S.; Chioti, A. A review of 3D printing techniques for bio-carrier fabrication. *J. Clean. Prod.* **2021**, *318*, 128469. [[CrossRef](#)]
10. Da Silva, C.; Astals, S.; Peces, M.; Campos, J.L.; Guerrero, L. Biochemical methane potential (BMP) tests: Reducing test time by early parameter estimation. *Waste Manag.* **2018**, *71*, 19–24. [[CrossRef](#)] [[PubMed](#)]
11. Christensen, G.D.; Simpson, W.A.; Younger, J.J.; Baddour, L.M.; Barrett, F.F.; Melton, D.M.; Beachey, E.H. Adherence of coagulase-negative staphylococci to plastic tissue culture plates: A quantitative model for the adherence of staphylococci to medical devices. *J. Clin. Microbiol.* **1985**, *22*, 996–1006. [[CrossRef](#)] [[PubMed](#)]
12. Janda, J.M.; Abbott, S.L. 16S rRNA Gene Sequencing for Bacterial Identification in the Diagnostic Laboratory: Pluses, Perils, and Pitfalls. *J. Clin. Microbiol.* **2007**, *45*, 2761–2764. [[CrossRef](#)] [[PubMed](#)]
13. Mandakhalikar, K.D.; Rahmat, J.N.; Chiong, E.; Neoh, K.G.; Shen, L.; Tambyah, P.A. Extraction and quantification of biofilm bacteria: Method optimized for urinary catheters. *Sci. Rep.* **2018**, *8*, 8069. [[CrossRef](#)] [[PubMed](#)]
14. Rice, E.W.; Baird, R.B.; Eaton, A.D. *Standard Methods for the Examination of Water and Wastewater*, 23rd ed.; American Public Health Association, American Water Works Association, Water Environment Federation: Alexandria, VA, USA, 2017.
15. Hwang, B.K.; Kim, J.H.; Ahn, C.H.; Lee, C.H.; Song, J.Y.; Ra, Y.H. Effect of disintegrated sludge recycling on membrane permeability in a membrane bioreactor combined with a turbulent jet flow ozone contactor. *Water Res.* **2010**, *44*, 1833–1840. [[CrossRef](#)] [[PubMed](#)]
16. Banti, D.C.; Karayannakidis, P.D.; Samaras, P.; Mitrakas, M.G. An innovative bioreactor set-up that reduces membrane fouling by adjusting the filamentous bacterial population. *J. Membr. Sci.* **2017**, *542*, 430–438. [[CrossRef](#)]
17. Dubois, M.; Gilles, K.A.; Hamilton, J.K.; Rebers, P.A.; Smith, F. Colorimetric Method for Determination of Sugars and Related Substances. *Anal. Chem.* **1956**, *28*, 350–356. [[CrossRef](#)]
18. Hartree, E. Determination of protein: A modification of the lowry method that gives a linear photometric response. *Anal. Biochem.* **1972**, *48*, 422–427. [[CrossRef](#)]
19. Bolyen, E.; Rideout, J.R.; Dillon, M.R.; Bokulich, N.; Abnet, C.C.; Al-Ghalith, G.A.; Alexander, H.; Alm, E.J.; Arumugam, M.; Asnicar, F.; et al. Reproducible, interactive, scalable and extensible microbiome data science using QIIME 2. *Nat. Biotechnol.* **2019**, *37*, 852–857. [[CrossRef](#)]
20. Callahan, B.J.; McMurdie, P.J.; Rosen, M.J.; Han, A.W.; Johnson, A.J.A.; Holmes, S.P. DADA2: High-resolution sample inference from Illumina amplicon data. *Nat. Methods* **2016**, *13*, 581. [[CrossRef](#)]
21. Quast, C.; Pruesse, E.; Yilmaz, P.; Gerken, J.; Schweer, T.; Yarza, P.; Peplies, J.; Glockner, F.O. The SILVA ribosomal RNA gene database project: Improved data processing and web-based tools. *Nucleic Acids Res.* **2013**, *41*, D590–D596. [[CrossRef](#)]
22. Duan, L.; Jiang, W.; Song, Y.H.; Xia, S.Q.; Hermanowicz, S.W. The characteristics of extracellular polymeric substances and soluble microbial products in moving bed biofilm reactor-membrane bioreactor. *Bioresour. Technol.* **2013**, *148*, 436–442. [[CrossRef](#)] [[PubMed](#)]
23. Nobu, M.K.; Narihiro, T.; Mei, R.; Kamagata, Y.; Lee, P.K.H.; Lee, P.H.; McInerney, M.J.; Liu, W.T. Catabolism and interactions of uncultured organisms shaped by eco-thermodynamics in methanogenic bioprocesses. *Microbiome* **2020**, *8*, 111. [[CrossRef](#)] [[PubMed](#)]
24. Ijoma, G.N.; Nkuna, R.; Mutungwazi, A.; Rashama, C.; Matambo, T.S. Applying PICRUSt and 16S rRNA functional characterisation to predicting co-digestion strategies of various animal manures for biogas production. *Sci. Rep.* **2021**, *11*, 19913. [[CrossRef](#)]
25. Wagner, M.; Loy, A.; Nogueira, R.; Purkhold, U.; Lee, N.; Daims, H. Microbial community composition and function in wastewater treatment plants. *Antonie Van Leeuwenhoek Int. J. Gen. Mol. Microbiol.* **2002**, *81*, 665–680. [[CrossRef](#)] [[PubMed](#)]
26. Tice, H.; Mayilraj, S.; Sims, D.; Lapidus, A.; Nolan, M.; Lucas, S.; Del Rio, T.G.; Copeland, A.; Cheng, J.F.; Meincke, L.; et al. Complete genome sequence of *Nakamurella multipartita* type strain (Y-104(T)). *Stand. Genom. Sci.* **2010**, *2*, 168–175. [[CrossRef](#)]
27. Zorz, J.K.; Kozłowski, J.A.; Stein, L.Y.; Strous, M.; Kleiner, M. Comparative Proteomics of Three Species of Ammonia-Oxidizing Bacteria. *Front. Microbiol.* **2018**, *9*, 938. [[CrossRef](#)]
28. Montalvo, S.; Huiliñir, C.; Borja, R.; Sánchez, E.; Herrmann, C. Application of zeolites for biological treatment processes of solid wastes and wastewaters—A review. *Bioresour. Technol.* **2020**, *301*, 122808. [[CrossRef](#)]
29. Montalvo, S.; Guerrero, L.; Borja, R.; Sánchez, E.; Milán, Z.; Cortés, I.; De La La Rubia, M.A. Application of natural zeolites in anaerobic digestion processes: A review. *Appl. Clay Sci.* **2012**, *58*, 125–133. [[CrossRef](#)]
30. Sudibyo, H.; Shabrina, Z.L.; Wondah, H.R.; Hastuti, R.T.; Purnomo, C.W.; Budhijanto, W. Anaerobic digestion of landfill leachate with natural zeolite and sugarcane bagasse fly ash as the microbial immobilization media in packed bed reactor. *Acta Polytech.* **2018**, *58*, 57–68. [[CrossRef](#)]
31. Andalib, M.; Elbeshbishy, E.; Mustafa, N.; Hafez, H.; Nakhla, G.; Zhu, J. Performance of an anaerobic fluidized bed bioreactor (AnFBR) for digestion of primary municipal wastewater treatment biosolids and bioethanol thin stillage. *Renew. Energy* **2014**, *71*, 276–285. [[CrossRef](#)]

32. Montalvo, S.; Gonzalez, P.; Mena, C.; Guerrero, L.; Borja, R. Influence of the food to microorganisms (F/M) ratio and temperature on batch anaerobic digestion processes with and without zeolite addition. *J. Environ. Sci. Health Part A* **2012**, *47*, 1785–1794. [[CrossRef](#)] [[PubMed](#)]
33. Andalib, M.; Hafez, H.; Elbeshbishy, E.; Nakhla, G.; Zhu, J. Treatment of thin stillage in a high-rate anaerobic fluidized bed bioreactor (AFBR). *Bioresour. Technol.* **2012**, *121*, 411–418. [[CrossRef](#)]
34. Li, R.; Liu, D.; Zhang, Y.; Zhou, J.; Tsang, Y.F.; Liu, Z.; Duan, N.; Zhang, Y. Improved methane production and energy recovery of post-hydrothermal liquefaction waste water via integration of zeolite adsorption and anaerobic digestion. *Sci. Total Environ.* **2019**, *651*, 61–69. [[CrossRef](#)] [[PubMed](#)]
35. Wijesinghe, D.T.N.; Dassanayake, K.B.; Sommer, S.G.; Scales, P.; Chen, D. Biogas improvement by adding Australian zeolite during the anaerobic digestion of C: N ratio adjusted swine manure. *Waste Biomass Valorization* **2019**, *10*, 1883–1887. [[CrossRef](#)]
36. Kotobuki, M. Properties of Al₂O₃ Pastes Using Inorganic Na₂SiO₃ Binder and Organic Binder for Direct Ink Writing. *Phys. Status Solidi B-Basic Solid State Phys.* **2022**, *259*, 2100520. [[CrossRef](#)]
37. Schwarz, J.A.; Contescu, C.; Contescu, A. Methods for Preparation of Catalytic Materials. *Chem. Rev.* **1995**, *95*, 477–510. [[CrossRef](#)]
38. Chen, S.J.; Zhu, M.; Fu, Y.; Huang, Y.X.; Tao, Z.C.; Li, W.L. Using 13X, LiX, and LiPdAgX zeolites for CO₂ capture from post-combustion flue gas. *Appl. Energy* **2017**, *191*, 87–98. [[CrossRef](#)]
39. Bernholc, J.; Brenner, D.; Nardelli, M.B.; Meunier, V.; Roland, C. Mechanical and electrical properties of nanotubes. *Annu. Rev. Mater. Res.* **2002**, *32*, 347. [[CrossRef](#)]
40. Aranzabal, A.; Iturbe, D.; Romero-Sáez, M.; González-Marcos, M.P.; González-Velasco, J.R.; González-Marcos, J.A. Optimization of process parameters on the extrusion of honeycomb shaped monolith of H-ZSM-5 zeolite. *Chem. Eng. J.* **2010**, *162*, 415–423. [[CrossRef](#)]
41. Jiang, Z.; An, N.; Chu, Y.; Cao, B.; Wu, F.; Zhang, Y.; Zhang, Y.; Li, Y.; Zhang, Y. Growth, biofilm formation and atrazine degrading gene (trzN) expression of *Arthrobacter* sp. DNS10 cultured with montmorillonite, kaolinite and goethite. *Chemosphere* **2022**, *307*, 135904. [[CrossRef](#)]
42. Zhang, Y.; Lu, C.; Chen, Z.; Song, Y.; Li, H.; Han, Y.; Hou, Y.; Guo, J. Multifaceted synergistic electron transfer mechanism for enhancing denitrification by clay minerals. *Sci. Total Environ.* **2022**, *812*, 152222. [[CrossRef](#)] [[PubMed](#)]
43. Xing, Y.; Luo, X.; Liu, S.; Wan, W.; Huang, Q.; Chen, W. Synergistic effect of biofilm growth and cadmium adsorption via compositional changes of extracellular matrix in montmorillonite system. *Bioresour. Technol.* **2020**, *315*, 123742. [[CrossRef](#)] [[PubMed](#)]
44. Cai, P.; Liu, X.; Ji, D.; Yang, S.; Walker, S.L.; Wu, Y.; Gao, C.; Huang, Q. Impact of soil clay minerals on growth, biofilm formation, and virulence gene expression of *Escherichia coli* O157:H7. *Environ. Pollut.* **2018**, *243*, 953–960. [[CrossRef](#)]
45. Song, Z.; Zhang, X.; Ngo, H.H.; Guo, W.; Song, P.; Zhang, Y.; Wen, H.; Guo, J. Zeolite powder based polyurethane sponges as biocarriers in moving bed biofilm reactor for improving nitrogen removal of municipal wastewater. *Sci. Total Environ.* **2019**, *651*, 1078–1086. [[CrossRef](#)]
46. Nguyen, T.M.; Ha, P.T.; Le, T.T.H.; Phan, K.S.; Mai, T.T.T.; Hoang, P.H. Modification of expanded clay carrier for enhancing the immobilization and nitrogen removal capacity of nitrifying and denitrifying bacteria in the aquaculture system. *J. Biosci. Bioeng.* **2022**, *134*, 41–47. [[CrossRef](#)]
47. Saidulu, D.; Srivastava, A.; Gupta, A.K. Enhancement of wastewater treatment performance using 3D printed structures: A major focus on material composition, performance, challenges, and sustainable assessment. *J. Environ. Manag.* **2022**, *306*, 114461. [[CrossRef](#)] [[PubMed](#)]
48. Wingender, J.; Neu, T.R.; Flemming, H.-C. What are Bacterial Extracellular Polymeric Substances? In *Microbial Extracellular Polymeric Substances*; Springer: Berlin/Heidelberg, Germany, 1999; pp. 1–19.
49. Lin, H.; Zhang, M.; Wang, F.; Meng, F.; Liao, B.-Q.; Hong, H.; Chen, J.; Gao, W. A critical review of extracellular polymeric substances (EPSs) in membrane bioreactors: Characteristics, roles in membrane fouling and control strategies. *J. Membr. Sci.* **2014**, *460*, 110–125. [[CrossRef](#)]
50. Lapidou, C.S.; Rittmann, B.E. A unified theory for extracellular polymeric substances, soluble microbial products, and active and inert biomass. *Water Res.* **2002**, *36*, 2711–2720. [[CrossRef](#)]
51. Liu, D.; Li, C.; Guo, H.; Kong, X.; Lan, L.; Xu, H.; Zhu, S.; Ye, Z. Start-up evaluations and biocarriers transfer from a trickling filter to a moving bed bioreactor for synthetic mariculture wastewater treatment. *Chemosphere* **2019**, *218*, 696–704. [[CrossRef](#)]
52. Lin, H.; Sun, S.; Lin, Z.; Chen, M.; Fang, L.; Ma, R.; Lin, J.; Luo, J. Bio-carrier-enhanced aerobic granulation: Effects on the extracellular polymeric substances production and microorganism community. *Chemosphere* **2021**, *280*, 130756. [[CrossRef](#)]
53. Wang, M.; Zhou, J.; Yuan, Y.-X.; Dai, Y.-M.; Li, D.; Li, Z.-D.; Liu, X.-F.; Zhang, X.-Y.; Yan, Z.-Y. Methane production characteristics and microbial community dynamics of mono-digestion and co-digestion using corn stalk and pig manure. *Int. J. Hydrogen Energy* **2016**, *42*, 4893–4901. [[CrossRef](#)]
54. Wang, H.; Tolvanen, K.; Lehtomäki, A.; Puhakka, J.; Rintala, J. Microbial community structure in anaerobic co-digestion of grass silage and cow manure in a laboratory continuously stirred tank reactor. *Biogeochemistry* **2009**, *21*, 135–146. [[CrossRef](#)] [[PubMed](#)]
55. Venkiteshwaran, K.; Milferstedt, K.; Hamelin, J.; Fujimoto, M.; Johnson, M.; Zitomer, D.H. Correlating methane production to microbiota in anaerobic digesters fed synthetic wastewater. *Water Res.* **2017**, *110*, 161–169. [[CrossRef](#)]

56. Yan, L.; Gao, Y.; Wang, Y.; Liu, Q.; Sun, Z.; Fu, B.; Wen, X.; Cui, Z.; Wang, W. Diversity of a mesophilic lignocellulolytic microbial consortium which is useful for enhancement of biogas production. *Bioresour. Technol.* **2012**, *111*, 49–54. [[CrossRef](#)] [[PubMed](#)]
57. Wang, M.; Zhang, X.; Zhou, J.; Yuan, Y.; Dai, Y.; Li, D.; Li, Z.; Liu, X.; Yan, Z. The dynamic changes and interactional networks of prokaryotic community between co-digestion and mono-digestions of corn stalk and pig manure. *Bioresour. Technol.* **2017**, *225*, 23–33. [[CrossRef](#)] [[PubMed](#)]
58. Ferry, J.G. Enzymology of one-carbon metabolism in methanogenic pathways. *Fems Microbiol. Rev.* **1999**, *23*, 13–38. [[CrossRef](#)]
59. Gao, Y.; Yang, A.; Bao, J.; Ma, R.; Yan, L.; Wang, Y.; Wang, W. Bioreactor performance and microbial community dynamics in a production-scale biogas plant in northeastern China. *Int. J. Agric. Biol. Eng.* **2017**, *10*, 191–201. [[CrossRef](#)]
60. Zhao, Y.; Xu, C.; Ai, S.; Wang, H.; Gao, Y.; Yan, L.; Mei, Z.; Wang, W. Biological pretreatment enhances the activity of functional microorganisms and the ability of methanogenesis during anaerobic digestion. *Bioresour. Technol.* **2019**, *290*, 121660. [[CrossRef](#)]
61. Wang, H.; Lim, T.T.; Duong, C.; Zhang, W.; Xu, C.; Yan, L.; Mei, Z.; Wang, W. Long-Term Mesophilic Anaerobic Co-Digestion of Swine Manure with Corn Stover and Microbial Community Analysis. *Microorganisms* **2020**, *8*, 188. [[CrossRef](#)]
62. Stepanov, V.G.; Xiao, Y.; Tran, Q.; Rojas, M.; Willson, R.C.; Fofanov, Y.; E Fox, G.; Roberts, D.J. The presence of nitrate dramatically changed the predominant microbial community in perchlorate degrading cultures under saline conditions. *BMC Microbiol.* **2014**, *14*, 225. [[CrossRef](#)]
63. Oren, A. The Family Rhodocyclaceae. In *The Prokaryotes: Alphaproteobacteria and Betaproteobacteria*; Rosenberg, E., DeLong, E.F., Lory, S., Stackebrandt, E., Thompson, F., Eds.; Springer: Berlin/Heidelberg, Germany, 2014; pp. 975–998.
64. Urakami, T.; Araki, H.; Oyanagi, H.; Suzuki, K.-I.; Komagata, K. *Paracoccus aminophilus* sp. nov. and *Paracoccus aminovorans* sp. nov., Which Utilize N,N-Dimethylformamide. *Int. J. Syst. Evol. Microbiol.* **1990**, *40*, 287–291. [[CrossRef](#)] [[PubMed](#)]
65. Zhang, J.; Zheng, J.W.; Liang, B.; Wang, C.H.; Cai, S.; Ni, Y.Y.; He, J.; Li, S.P. Biodegradation of Chloroacetamide Herbicides by *Paracoccus* sp. FLY-8 in Vitro. *J. Agric. Food Chem.* **2011**, *59*, 4614–4621. [[CrossRef](#)] [[PubMed](#)]
66. Jenkins, D.; Richard, M.G.; Daigger, G.T. *Manual on the Causes and Control of Activated Sludge Bulking, Foaming and Other Solids Separation Problems*; IWA Publishing: London, UK, 2003.
67. Dubinina, G.; Savvichev, A.; Orlova, M.; Gavrish, E.; Verbarq, S.; Grabovich, M.; Dubinina, G.; Savvichev, A.; Orlova, M.; Gavrish, E.; et al. *Beggiatoa leptomitiformis* sp. nov., the first freshwater member of the genus capable of chemolithoautotrophic growth. *Int. J. Syst. Evol. Microbiol.* **2017**, *67*, 197–204. [[CrossRef](#)] [[PubMed](#)]
68. Schwedt, A.; Kreutzmann, A.-C.; Polerecky, L.; Schulz-Vogt, H.N. Sulfur Respiration in a Marine Chemolithoautotrophic *Beggiatoa* Strain. *Front. Microbiol.* **2012**, *2*, 276. [[CrossRef](#)]
69. Shintani, T.; Liu, W.T.; Hanada, S.; Kamagata, Y.; Miyaoka, S.; Suzuki, T.; Nakamura, K. *Micropruina glycogenica* gen. nov., sp. nov., a new Gram-positive glycogen-accumulating bacterium isolated from activated sludge. *Int. J. Syst. Evol. Microbiol.* **2000**, *50*, 201–207. [[CrossRef](#)]
70. Wang, R.; Peng, Y.; Cheng, Z.; Ren, N. Understanding the role of extracellular polymeric substances in an enhanced biological phosphorus removal granular sludge system. *Bioresour. Technol.* **2014**, *169*, 307–312. [[CrossRef](#)]
71. Basuvaraj, M.; Fein, J.; Liss, S.N. Protein and polysaccharide content of tightly and loosely bound extracellular polymeric substances and the development of a granular activated sludge floc. *Water Res.* **2015**, *82*, 104–117. [[CrossRef](#)]